Arrested development – a comparative analysis of multilayer corona textures in metamorphic rocks

Paula P. Ogilvie[1], Roger Lawrence R.L. Gibson[1],

[1]School of Geosciences, University of the Witwatersrand, P O WITS, Johannesburg 2050, South Africa

5 *Correspondence to*: Roger L. Gibson (roger.gibson@wits.ac.za)

Abstract. Coronas, including symplectites, are vital clues to the presence of arrested reaction and preservation of partial equilibrium in metamorphic and igneous rocks. Compositional zonation across such coronas is common, indicating the persistence of chemical potential gradients and incomplete equilibration. Major controls on corona mineralogy include *P, T* and *a*H2O during formation, continuous or non-continuous corona formation, reactant bulk compositions and extent of

10 metasomatic exchange with the surrounding rock, ~~relative diffusion rates for major components~~, and/or contemporaneous deformation and strain. High-variance local equilibria in a corona and disequilibrium across the corona as a whole preclude the application of conventional thermobarometry when determining *P-T* conditions of corona formation, and zonation in phase composition across a corona should not be interpreted as a record of discrete *P-T* conditions during successive layer growth along the P-T path. Rather, the local equilibria between mineral pairs in corona layers more likely reflect

15 compositional partitioning of the corona domain during steady-state growth at constant *P* and *T*.

Corona formation in pelitic and mafic bulk rock compositions requires dry, restitic bulk rock compositions. Since most melt is lost at or near peak conditions only a fraction of melt is retained in the restitic post-peak assemblage. Reduced melt volumes with cooling limit length-scales of diffusion to the extent that diffusion-controlled corona growth occurs. On the prograde path, the low melt (or melt-absent) volumes required for kinetically-constrained corona growth are only commonly

20 realised in mafic rocks, owing to their intrinsic anhydrous bulk composition, and in dry, restitic pelitic compositions that have lost melt in an earlier metamorphic event. Mafic and pelitic prograde coronas show similar ranges of thickness and vermicule size; prograde contact aureole coronas display similar thicknesses but slightly longer vermicule lengths compared to regional metamorphic coronas. Retrograde coronas in mafic rocks are significantly thinner than pelitic coronas and have smaller vermicule lengths, whereas retrograde pelitic coronas show similar parameters to their prograde counterparts.

25 Reduced maximum corona thickness and smaller maximum vermicule size in retrograde mafic coronas compared to retrograde pelitic coronas attests to more restricted length-scales of diffusion in melt-poor, anhydrous, mafic bulk rock compositions. Increased maximum layer thickness and vermicule size in prograde mafic coronas compared to retrograde mafic coronas is due to greater length-scales of diffusion in more melt-rich bulk compositions with protracted reaction along the prograde path. Prograde pelitic coronas do not differ significantly from retrograde pelitic coronas with respect to

microstructure, owing to the intrinsically more hydrous pelitic bulk compositions and capacity to generate diffusion-enhancing melt during decompression.

Through the application of either quantitative physical diffusion modelling of coronas or phase equilibria modelling utilising calculated chemical potential gradients, it is possible to model the evolution of a corona through *P-T-X* space by continuous or non-continuous processes. Since corona modelling employing calculated chemical potential gradients assumes nothing about the sequence in which the layer forms and is directly constrained by phase compositional variation within a layer, it allows far more nuanced and robust understanding of corona evolution and its implications for the path of a rock in *P-T-X* space.

Key words: corona, chemical potential gradient, diffusion, disequilibrium, metamorphism, mineral compositional zoning, reaction dynamics, reaction texture, symplectite.

1 Introduction

Fundamental to the study of metamorphic rocks is the application of equilibrium thermodynamics in the understanding of the development of a mineral assemblage within evolving pressure (*P*), temperature (*T*) and chemical potential regimes. In an equilibrated assemblage, the chemical potentials of all components are equal spatially throughout the equilibrium volume; however, different rates of intergranular diffusion for major and trace components limit the capacity of a rock to fully eliminate gradients in chemical potentials and attain equilibrium on both micro- and macro-scales (Carlson, 2002; White et al., 2008; White & Powell, 2011). A more realistic model of *partial equilibrium*, i.e., equilibrium for some components and not for others, is likely to be attained in a rock. In a sense partial equilibrium is fortuitous, since evidence of disequilibrium preserved in reaction textures reveals basic physico-chemical reaction dynamics operating during metamorphism that are obscured if a rock equilibrates completely. However, partial disequilibrium also compromises petrographic and geothermobarometric evidence as records of the metamorphic evolution of a rock and can lead to erroneous interpretations (White & Powell, 2011). An understanding of how partial equilibrium manifests petrographically and chemically is, thus, critical in refining our appreciation of metamorphic rocks.

The most obvious manifestation of partial equilibrium is that exhibited in reaction textures comprising coronas and symplectites. The spatially segregated phases preserved within these incipient reaction textures are the best petrographic evidence available to us to allow the study of the evolution of chemical potential gradients governing the reorganization of components within a rock with changing *P-T-X* (composition) conditions (e.g., White et al., 2008; Štípská, et al., 2010; White & Powell 2011; Baldwin et al., 2015). The disequilibrium commonly preserved in coronas and symplectites does not, however, preclude the application of equilibrium thermodynamics in modelling and interpreting those textures; it only invokes a reconsideration of the appropriate equilibration volume in which chemical potential gradients are absent (White & Powell, 2011). Within any reaction texture, at an appropriate scale, chemical equilibrium exists and attendant chemical

potentials may be determined for a given *P* and *T* within the local bulk composition dictated by the equilibration volume. This concept of local equilibrium was first introduced by Korzhinski (1959) and has been the premise upon which all studies of reaction textures are predicated.

In this paper, we present an analysis of more than 50 metamorphic corona textures (Appendices 1 and 2) and discuss two
5   contrasting modelling methodologies used in interpreting the evolution of these textures. We review recent strides in modelling corona textures utilising calculated phase diagrams and assess their significance and limitations when used to infer the *P-T-X* evolution of metamorphic rock.

2 Reaction kinetics and coronas

Metamorphic reactions are initiated when a pre-existing mineral assemblage becomes unstable owing to changing *P-T-X*
10   conditions, and seeks to re-establish chemical equilibrium by rearrangement of its chemical constituents into a new mineral assemblage. The critical kinetic constraints on extent of any metamorphic reaction are (a) the rate of supply of matter through intergranular diffusion; (b) the rate of reactant dissolution and product nucleation during recrystallisation (interface control); and (c) the rate of supply or removal of heat (Fisher, 1977; Joesten, 1977; Brady, 1983; Tracey and McLellan, 1985; Carlson, 2002). Interface reaction rate, in turn, depends on the affinity for reaction, i.e., the difference between the
15   chemical potentials of diffusing components and their equilibrium values (Carlson, 2002). The slowest of these rate-limiting processes determines the nature and extent of reaction and equilibration. During stages of reaction at high temperatures in the presence of a melt or fluid phase, reaction rates are typically interface- rather than diffusion-controlled since diffusion coefficients are large and, thus, unlikely to be rate-limiting. With cooling or loss of the melt or fluid phase, diffusion rates become more important, as does heat flux out of the system. Lower diffusion rates impede efficient chemical communication
20   of requisite components to reaction sites; consequently, the bulk rock composition becomes effectively partitioned into smaller compositional domains that are in local equilibrium, with gradients in chemical potential existing between them.

Multilayer coronas involving the spatial segregation of reaction products in layered corona bands arranged in order of increasing or decreasing chemical potential (Fisher, 1977; Joesten, 1977) are the most obvious manifestation of diffusion-controlled reactions. As changing *P* and *T* induces incipient reaction between contiguous metastable reactants, components
25   will start to migrate between the reactants. If the major components display variable intergranular diffusivities, they will be partitioned into a continuum of compositional subdomains, or incipient "effective bulk compositions", in each of which local equilibrium is attained with its own unique chemical potentials. The width of the corona and each of its layers will be dictated by the different length-scales of diffusion for each component. A layered corona assemblage develops, across which transient chemical potential gradients exist, which drive diffusion through the layers. With prolonged reaction or enhanced
30   intergranular diffusion, component flux through the corona layers equalises chemical potentials at all points in the corona. Local incipient bulk compositions of subdomains gradually should expand with mass transfer across layers and approach the

final steady-state effective bulk composition for the corona as a whole. Equilibrium is attained when no chemical potential gradients exist for any components, despite the spatial segregation of corona phases in layers.

The interpretation of corona textures has traditionally been a primary diagnostic tool for inferring metamorphic *P-T-t* paths and, hence, tectonics (Whitney and McLelland, 1973; Grew, 1980; Joesten, 1986; Droop, 1989; Clarke et al., 1989; Ashworth et al., 1992; White and Clarke, 1997; Norlander et al., 2002; White et al., 2002; Kelsey et al., 2003b; Johnson et al., 2004; Tsunogae and Van Reenen, 2006; Zulbati and Harley, 2007; Hollis et al., 2006). Kinetically constrained conditions may arise on both the prograde and retrograde path but, typically, coronas are thought to ~~have formed~~ during retrogression from peak *P-T* conditions as univariant, or at least very low variance, equilibria are crossed. The topology of the inferred univariants with respect to the peak assemblage has commonly been used to constrain a retrograde *P-T* path (Harley, 1989). Retarded reaction progress under retrograde conditions owing to sluggish reaction kinetics manifests as incomplete reaction between peak phases to produce layered, finely crystalline, spatially segregated reaction products, which armour the peak phases from further reaction.

The inherent assumption of disequilibrium between reactants and corona products was elegantly questioned in a study by White et al. (2002) on metapelites from the Musgrave Block in Australia. Phase equilibria modelling employing pseudosections in KFMASHTO demonstrated that corona textures could realistically be developed in a peak, high variance, assemblage that remains in equilibrium but undergoes large changes in mineral modes as the *P-T* path tracks through the phase field. Thus, it may not be necessary to invoke crossing of univariants and disequilibrium to explain corona textures. Indeed, the amount of decompression required to generate the equilibrium reaction texture described by White et al. (2002) was comparatively minor and may well have been overestimated by earlier workers (Harley, 1989). White & Powell (2011), ==also urge caution in assuming incomplete reaction progress in coronas where the cessation of textural development reflects the consumption of melt, in which case the reaction responsible has gone to completion.==

Whilst there is a general understanding of the processes that induce corona formation (e.g., Harley, 1989; White et al., 2002; Johnson et al., 2004; White et al., 2008), the mechanism for corona development is poorly known since the final steady-state configuration of corona layers observed in a rock reflects the complex evolution of chemical potential relationships with *P, T* and bulk composition. These same complexities must also govern metamorphic processes on the prograde path at larger scales. However, greater melt or fluid volumes and increasing temperatures on the prograde path facilitate equalisation of chemical potentials through ~~accelerated diffusion in~~ the assemblage, such that only the spatial sequestration of phases (for example, between melt-rich leucosomes and melt-poor mesosomes) attests to the compositional partitioning of the rock and attendant chemical potential gradients that must have prevailed during diffusion-controlled reaction (White et al., 2004). ~~In coronas, disequilibrium is frozen in the rock, preserving incipient reaction textures. They are, therefore, the best petrographic evidence available to us to allow the study of the evolution of chemical potential gradients governing the reorganization of components within a rock with changing~~ *P-T-X* ~~conditions (e.g., White et al., 2008).~~

3 Corona growth models

Two distinct ==paradigms== have evolved in the last four decades to explain development of multi-layered coronas, namely, synchronous, *continuous, single-stage, steady-state* (e.g., Ashworth and Sheplev, 1997) and *non-continuous, sequential* (Joesten 1986; White and Clarke, 1997) diffusion-controlled growth. ==Distinguishing between the two mechanisms for corona==

5 ==formation is critical when inferring information regarding the *P-T* path from them (White & Powell, 2011).==

3.1 Continuous, single-stage, steady-state, diffusion-controlled corona growth ~~(SSDC)~~

~~The~~ ~~single-stage, steady-state multilayer~~ growth model attributes corona development to diffusion-controlled reaction mechanisms at constant pressure and temperature, ~~with~~ local equilibrium and chemical potential gradients across each layer and the corona as a whole (Fig. 1). The spatial segregation of phases into layers reflects relative mobility of components

10 ~~owing to variable intergranular diffusivities~~ rather than distinct *P-T* conditions. All layers in the reaction bands coexist contemporaneously with infinitesimal thickness at the incipient stages of reaction. Only layer thickness increases with reaction duration and no change to the ==internal structure of the corona== occurs. Chemical potential gradients evolve toward a steady-state ~~and constant~~ final configuration balancing the rate of production and consumption of each component within each layer (Korzhinskii, 1959; Joesten, 1977; Mongkoltip and Ashworth, 1983; Foster, 1986; Grant, 1988; Johnson and

15 Carlson 1990; Carlson and Johnson, 1991; Ashworth and Birdi, 1990; Ashworth et al., 1992; Ashworth and Sheplev, 1997; Markl et al., 1998; Ashworth et al., 1998).

Figure 1 ~~demonstrates~~ incipient stages of SSDC corona formation chemographically and in chemical potential space by considering two phases (A and D) initially at equilibrium under P_1 and T_1 with bulk composition indicated by the circle (Fig. 1a). If new *P* and T conditions (P_2, T_2) ==are kinetically inhibited== and reaction progress becomes diffusion-controlled, relative

20 differences in intergranular diffusivities partition the original bulk composition (circle) into two ~~endmember~~, non-overlapping, local bulk compositions (square, triangle) ~~intermediate between the reactant compositions~~ (Fig. 1b). The product mineral assemblage layers are spatially segregated in local equilibrium and comprise the mineral assemblage stabilised in each local effective bulk composition, ~~i.e., the local bulk composition indicated by the square stabilises~~ ~~assemblage BCD and, similarly, the bulk composition indicated by the triangle stabilises assemblage ABC~~ (Fig. 1b). A

25 ternary *G-X* surface (Fig. 1c) indicates that the tangent planes to the minimum free energy assemblages have different orientations and, accordingly, components have different chemical potentials in each assemblage. The coexistence of two local juxtaposed equilibria buffers the chemical potentials of diffusing components across the coronas (Joesten, 1977). Figure 1d represents the associated isothermal-isobaric chemical potential saturation surface for each of the local phase assemblages (modified after Joesten, 1977). Each local bulk composition, represented by a three-phase assemblage, is

30 invariant in chemical potential space at constant *P* and *T*. The invariant assemblage ABC (triangle) lies at a higher chemical potential for component 3 and lower chemical potentials for components 1 and 2, than does the invariant assemblage BCD represented by the square. A projection of the saturation surface on the μ_{comp1}-μ_{comp2} plane ~~(Fig. 1e)~~ more clearly indicates

the difference between chemical potentials for each local equilibrium. Maintenance of these local equilibria requires that chemical potential gradients must exist across each layer and, thus, that the system as a whole is in disequilibrium, which drives diffusion of components from one compositional domain to another. ~~Chemical potential differences across each layer adjust to steady-state values that balance the rates of production and consumption of each component within the layer (Joesten, 1977).~~ Chemical potential gradients for rapidly diffusing components may be eliminated across the corona, whilst those for the slowest moving components (typically Al and Si) are maintained, establishing partial equilibrium.

Continued corona evolution entails the growth of a layer assemblage at the expense of its neighbour ~~by reaction with the diffusing components~~ (Joesten, 1977). The relative diffusive fluxes of components in adjacent layers determine which mineral phases are consumed and produced at each layer boundary, as well as the reaction stoichiometry (Joesten, 1977; Fisher, 1977). All mineral layers grow ~~at the same time,~~ by a set ~~of diffusion-controlled~~ reactions at layer ~~contacts, which~~ liberate and consume components in the appropriate proportions ~~to account for mass balance in the overall system~~ (Joesten, 1977, 1986; Fisher, 1977). The only layer that grows at both contacts is the layer that initially contained the original reactant interface (Joesten, 1977; Joesten, 1986). Fisher (1973) demonstrated that diffusion will automatically tend to shift potentials toward values such that the flux differences at every point in a corona balance local reactions, thereby establishing a steady-state configuration. Growth of coronas will ~~slow~~ and eventually cease ~~either when diffusion paths become too tortuous and long; chemical potential gradients approach values too low to drive significant diffusion; and/or intergranular diffusivities are reduced with cooling during retrogression~~ (Joesten, 1977; Fisher, 1977; Ashworth and Sheplev, 1997).

The corona in Fig. 2 is a schematic reconstruction of those described by Johnson and Carlson (1990) from metagabbros in the Adirondack Mountains that they interpreted as a natural example of ~~single-stage, steady-state, diffusion-controlled growth at constant *P* and *T*. During granulite facies metamorphism a~~ primary igneous assemblage involving contiguous olivine and plagioclase (Fig. 2a) becomes unstable and is replaced by a new stable assemblage including orthopyroxene, clinopyroxene, plagioclase and garnet (Fig. 2b). ~~As rates of *P-T* change exceed rates of intergranular diffusion in the dry mafic bulk composition, diffusion-controlled reaction ensues.~~ Variable relative rates of intergranular diffusion manifest as spatially segregated product layers, depending on the diffusion range of each component, and the corona domain is partitioned into a continuum of compositional subdomains or incipient effective bulk compositions in which local equilibrium is attained, each with unique chemical potentials (Fig. 1). Since Al is the slowest-diffusing component, the most aluminous product phase adjoins the most aluminous reactant and asymmetric composition profiles for slower-diffusing species are established across product bands, e.g., Al content in product bands increases toward the Al-rich reactant. Fe, Mg and Si released from olivine diffuse down chemical potential gradients toward plagioclase, whereas Na, Ca, Al and Si released from plagioclase diffuse toward olivine. Reactions occur at layer ~~boundaries~~ and layers expand as ~~diffusion~~ progresses (Fig. 2b). ~~The width and composition of each corona layer depend on the relative fluxes of the diffusing elements.~~ Inherent in the model is that the product mineral assemblage does not change as reaction proceeds. With time, chemical

potentials and fluxes approach steady-state values. Mg, Ca, Na and Al are imported into the corona and Fe and Si are exported from the corona. Minor spinel clouding occurs in reactant plagioclase as Ca and Si diffuse preferentially into the reaction band, creating a Si deficiency that stabilises spinel in relict reactant plagioclase (Johnson and Carlson, 1990).

3.2 Non-continuous, sequential, diffusion-controlled corona growth

5 ~~The~~ sequential, diffusion-controlled corona ~~layer~~ growth model involves successive, step-wise, growth of layers, leading to overprinting and partial re-equilibration of younger ~~corona~~ layers as new equilibria are encountered on either the prograde or retrograde path. These changes are typically triggered by changing P and/or T but can also be triggered through changing component fluxes through the corona as a function of evolving local effective bulk compositions (e.g., Griffin, 1972; Griffin and Heier, 1973; Joesten, 1986; Droop, 1989; Indares, 1993; White et al., 2002; Johnson et al., 2004; Štípská et al., 2010;
10 Baldwin et al, 2015). In contrast to the single-stage, steady-state model, the internal layer configuration of the corona reaction band evolves with time as new layers develop and old layers are resorbed. Relative diffusion fluxes and attendant chemical potential differences shift and evolve from one steady-state configuration to another under new *P-T-X* conditions.

Sequential corona development with changing P and T has been demonstrated in prograde coronas in mafic rocks between olivine and plagioclase by Griffin (1972). He derived a sequential model for corona formation that involved cooling from
15 igneous temperatures at between 8 and 11 kbar and crossing of univariant equilibria (Figs. 3 and 4). Initially, olivine and plagioclase crystallised at point A, but as the rock cooled, it was buried and followed the path delineated by the arrow in Fig. 4. At point B, the olivine and plagioclase reacted to produce Tschermakitic clinopyroxene (Cpx I) and aluminous orthopyroxene (Opx I; Fig. 3a). Phases in all diagrams and text are labelled using Kretz (1983) mineral abbreviations. As the rock tracked through *P-T* space from B to C (Fig. 4), the ~~clinopyroxene (Cpx I)~~ exsolved spinel and anorthite to form a less
20 Tschermakitic ~~clinopyroxene~~ (Cpx II; Fig. 3b). This clinopyroxene was partly consumed at point C (Fig. 4) to produce garnet and a jadeitic clinopyroxene (Cpx III; Fig. 3c). Further cooling into the eclogite facies produced omphacitic clinopyroxene and garnet with lesser quartz at point D (Fig. 3d). Finally, decompression on exhumation induced the exsolution of the jadeite component from omphacite to yield diopside (Cpx IV) and plagioclase towards point E (Figs. 3e and 4).

25 ~~Mork (1986) also invoked a sequential model for corona formation between olivine and plagioclase in western Norway as a result of a clockwise *P-T* path.~~

Sequential corona development may also occur at constant P and T with changing component fluxes across the corona band. A multilayer corona may evolve in a steady or quasi-stationary state controlled by diffusion (single-stage, steady-state growth) and then subsequently modify through back-reaction between two adjacent layers at constant P and T through
30 changing composition of the effective equilibration volume as the composition of a reactant evolves with protracted reaction. Brady (1977) and Vidale (1969) introduced a modification to the steady-state model that was first used to explain corona

variability by Johnson and Carlson (1990). Vidale (1969) modelled the development of calc-silicate bands in a system with waning availability of certain components. According to his model, rapidly diffusing components in a reaction band will eventually eliminate their chemical potential gradients. The chemical potentials of those rapidly diffusing components are then determined by equilibria outside of the corona band. As the number of components exerting a diffusive control on the

5   reaction is reduced by one, so one mineral phase is lost from the band (Vidale, 1969, Brady, 1977). This manifests as 'cannibalisation' of corona layers comprising the rapidly diffusing components. The original steady state is modified as the system enters a transient state that will evolve through time toward a new steady state with constant chemical potential gradients.

Johnson and Carlson (1990) employed the sequential development model to explain the variability in corona product

10 assemblages developed between plagioclase and olivine in a mafic granulite from the Adirondack Mountains (Fig. 5). As the reactant plagioclase was gradually exhausted in Ca and Si, it was converted from labradorite to andesine + spinel (Fig. 5a). This modification of the chemical potentials of Ca and Si by equilibria outside of the corona band manifests as the destabilisation and subsequent 'cannibalisation' of, first, the plagioclase corona layer and then the clinopyroxene layer (Fig. 5a, b), as the system evolved toward a new steady-state scenario with constant chemical potential gradients. According to

15 Johnson and Carlson (1990), all corona bands were initially plagioclase- and clinopyroxene-bearing, but then evolved to different final configurations with greater or lesser cannibalisation of these phases, depending on the availability of Ca and Si in the surrounding phases. Where the olivine grain adjoins the spinel-poor plagioclase (originally less calcic, An$_{43}$), both product plagioclase and clinopyroxene have been consumed, and the orthopyroxene is in contact with garnet (Fig. 5b, c). In contrast, where olivine is adjacent to spinel-rich reactant plagioclase (originally more calcic, An$_{56}$), corona plagioclase and

20 clinopyroxene are retained (Fig. 5c).

Sequential layer development in a corona through variation of P, T and changing bulk composition of the corona reaction volume was invoked by Indares (1993) to explain coronas between olivine and plagioclase in an olivine gabbro from the Shabogamo Intrusive Suite, Eastern Grenville Province. Initially, at high P and T, under eclogite facies conditions, calcic plagioclase reacted with olivine to form orthopyroxene and garnet coronas (Fig. 6a). The relative difference in intergranular

25 diffusivities of components manifests as two distinct corona layers over which chemical potential gradients exist, grading from aluminous garnet adjacent to plagioclase to Al-poor orthopyroxene adjacent to olivine. Excess Al in the plagioclase was accommodated by the formation of corundum (Fig. 6a). At the same pressure and temperature, the garnet layer grew by reaction between calcic plagioclase and corona orthopyroxene in a local effective bulk composition different from that which produced the initial corona orthopyroxene and garnet, which included olivine (Fig. 6b). Continued reaction generated excess

30 Si and Al in the reactant plagioclase, which reacted with corundum to form kyanite (Fig. 6b). In Fig. 6c, the reactant plagioclase is relatively enriched in Na through the two former reactions. Na then diffused out of plagioclase and reacted with corona orthopyroxene and garnet to form omphacite. In response, more kyanite formed in the plagioclase to

accommodate excess residual Si and Al. With subsequent exhumation and decompression, corona garnet reacted with kyanite and corundum in plagioclase to form spinel and more calcic plagioclase (Fig. 6d). In addition, garnet reacted with omphacite and some excess Si to produce intervening plagioclase.

The sequential development of symplectites in pelitic rocks has been elegantly modelled using calculated phase diagrams involving chemical potentials for coupled spinel+plagioclase symplectites and monomineralic plagioclase coronas after kyanite by Štípská et al. (2010) and Baldwin et al. (2015). With isothermal decompression from peak conditions, kyanite is no longer stable and a zoned monomineralic plagioclase layer forms between the kyanite and matrix with quartz in excess and only Al_2O_3 considered immobile. As the plagioclase layer evolves, the diffusion of SiO_2 through the plagioclase layer from the matrix is retarded and the local equilibrium volume encompassing the kyanite and plagioclase layer contact becomes a silica-deficient one. The chemical potential of SiO_2 at the kyanite contact is accordingly lowered sufficiently to stabilise spinel symplectitically intergrown with plagioclase.

4 Controls on corona development in granulites

Of all the substantive literature references to corona textures, only a few do not relate to pelitic or mafic bulk compositions. Appendix 1 presents details of prograde coronas in the literature, whereas Appendix 2 comprises a selection of the more numerous references to coronas formed during retrograde re-equilibration. Selected coronas from mafic and pelitic rocks are schematically illustrated in Figures 7 and 8, respectively. The assemblages and microstructure in coronas in both pelitic and mafic rocks vary considerably depending on (a) metamorphic conditions (*P, T* and aH$_2$O), (b) formation mechanism through either steady-state or sequential layer development, (c) reactant compositions, (d) diffusion kinetics, and (e) the amount of deformation or strain intensity on either the prograde or retrograde path.

4.1 Pressure, temperature and aH$_2$O

Pressure, temperature and aH$_2$O conditions determine which mineral phases ~~manifest~~ in the corona. In olivine gabbros or troctolites from the Adirondack Highlands, coronal assemblages vary from *Ol*│Opx+Cpx│Grt│*Pl* (reactants in italics; ~~abbreviations after Kretz, 1983~~) in the northeast (Johnson and Carlson, 1990 – Fig. 5a) to *Ol*│Opx│Cpx+Spl│*Pl* in the southwest (Whitney and McLelland, 1973 – Fig. 7a), with the presence of garnet in the former being attributed to higher pressures towards the northeast. In the Newer Basic Intrusion of NE Scotland, the coronal assemblage *Ol*│Opx│Hbl+Spl│*Pl* is observed (Mongkoltip and Ashworth, 1983 – Fig. 7b). In this case, Hbl is favoured over Cpx under higher aH$_2$O conditions. Similarly, the dominance of hornblende in the corona assemblage between garnet and clinopyroxene described in Carlson and Johnson (1991) (Fig. 7c) versus the restriction of pargasite to the layer closest to garnet in the coronas described by Baldwin et al. (2004) (Fig. 7d), is attributed to higher aH$_2$O in the former corona compositional domain.

In metapelites, coronas after sapphirine and quartz comprise the sequence $Spr│Sil│Opx│Qtz$ at higher pressures, but $Spr│Sil│Opx+Crd│Qtz$ at lower pressures and temperatures and/or higher aH_2O conditions (e.g., Lal et al., 1987). Coronas after gedrite and kyanite from the Thor Odin Dome in British Columbia comprise the sequence $Ged│Crd│Crd+Spl$ symplectite│Crd+Crn symplectite│Ky (Norlander et al., 2002 – Fig. 8a). The lower-temperature equivalent corona

5 (assuming minimal bulk compositional differences) is $Ged│Crd│St│Ky$, which is seen in the Errabiddy metapelitic granulites in Western Australia (Baker et al., 1987).

4.2 Sequential versus single-stage corona formation mechanism

Corona assemblages are also governed by the mechanism by which they formed, i.e., either in a single-stage, steady-state event, or as sequential layers in response to varying pressure, temperature or component fluxes into the reaction volume.

10 Johnson and Carlson (1990) characterised a range of corona textures between olivine and plagioclase in the Adirondacks, New York (Fig. 2 and Fig. 5) and attributed different corona configurations to varying extents of internal corona cannibalisation with waning Ca and Si fluxes across the corona depending on the original composition of the plagioclase reactant. Alternatively, intervening layers may develop with cooling as length-scales of diffusion become more constrained and the corona compositional domain partitions into smaller-volume local equilibria in which a secondary corona

15 assemblage may develop by reaction between two contiguous layers at new P and T conditions (e.g., Griffin, 1972; Brandt et al., 2003). Most coronas listed in Appendices 1 and 2 appear to be interpreted via the single-stage, steady-state model, but sequential growth models are relatively common.

Determining which model of corona formation is applicable in a specific context is commonly difficult but vital if information on the P-T path is to be gleaned correctly from the corona (White and Clarke, 1997). This is critically evident in

20 contrasting interpretations of the coronas formed between olivine and plagioclase in metagabbros from Risor, Norway (Joesten, 1986; Ashworth, 1986).

Joesten (1986) cited textural evidence and the diffusional instability of any closed-system, steady-state, diffusion model for the coronas in support of a model involving a primary magmatic origin for the coronas, followed by secondary annealing. He suggested that cuspate olivine-orthopyroxene contacts, thickening of orthopyroxene layers at narrow terminations of olivine

25 grains, irregular contacts between orthopyroxene-spinel and amphibole-spinel layers, and sectoral heterogeneity in the corona assemblage depending on the adjacent magmatic phase (i.e., either plagioclase, amphibole or clinopyroxene) are all inconsistent with a diffusion-controlled origin. He suggested these features were more likely a result of olivine dissolution in a melt, followed by the sequential growth of corona layers with cooling at magmatic temperatures above the olivine-plagioclase stability field. Joesten (1986) proposed that these primary magmatic coronas were diffusionally unstable and that

30 they were spontaneously partially to completely annealed on cooling.

In contrast, Ashworth (1986) suggested the Risor coronas formed by single-stage, steady-state, diffusion-controlled replacement of plagioclase and olivine with an open-system modification to mass-balance model constraints. Textural evidence apparently inconsistent with a diffusion model was attributed to locally variable kinetic controls on reaction mechanism, for example, epitaxial growth of tabular amphibole on magmatic grains versus heterogeneous nucleation at

5 reactant contacts. Ashworth (1986) did not address the sectoral heterogeneity of the coronas nor the irregular contacts between amphibole-spinel and orthopyroxene-spinel layers; however, it is conceivable that variation in the bulk composition of the equilibration volume - both spatially and temporally as reaction proceeded - may account for such heterogeneity (e.g., Johnson and Carlson 1990).

Alternative sequential models of corona formation, invoking varying *P, T* and/or boundary fluxes, may ~~similarly~~ have

10 important implications for reconstruction of *P-T* paths. For the same corona textures between olivine and plagioclase in the New York Adirondacks (Figs. 2, 5, and 6), three different *P-T* paths were constructed by Griffin (1972), Johnson and Carlson (1990) and Indares (1993), respectively, based on their inferences about the drivers behind the corona reactions, namely, changing pressure and temperature (Griffin, 1972; Joesten, 1986), changing component fluxes (Johnson and Carlson, 1990), or a combination of all three parameters (Indares, 1993). Mass-balance constraints and compositional

15 zonation within each corona assemblage were cited in each case in support of the adopted model. Johnson and Carlson (1990) attributed different corona configurations to varying extents of internal corona cannibalisation with waning Ca and Si fluxes across the corona that were dependent on the original composition of the plagioclase reactant. Alternatively, intervening layers may develop on a more local scale with cooling as ==length-scales of diffusion become more constrained and the corona compositional domain partitions into smaller-volume local equilibria in which a secondary corona==

20 ==assemblage may develop by reaction between two contiguous layers at new *P* and *T* conditions== (e.g., Griffin, 1972; Brandt et al., 2003).

Criteria for the identification of single-stage, steady-state layer growth include mineral zonation and a marked spatial organisation of product reaction bands such that each layer represents a 'non-overlapping volume in compositional space' (Joesten, 1977; Fisher, 1977), all arranged in an orderly sequence of increasing or decreasing chemical potential (Fisher,

25 1977). If the corona has not attained equilibrium, asymmetric composition profiles in minerals within a corona layer and in the corona as a whole are consistent with chemical potential gradients induced by relative differences in intergranular diffusion rates of components at approximately constant *P-T* conditions (Indares, 1993, White and Clarke, 1997). In contrast, a sequential corona model predicts symmetric, radial zoning of phases with respect to grain boundaries. Mass balance constraints commonly preclude the formation of an intervening layer by reaction between two initially contiguous layers in a

30 sequential model. This necessitates the diffusion of requisite components from outside the limits of the immediate equilibration volume within a single-stage, steady-state diffusional regime. Even so, evidence may be equivocal and it may not be possible to exclusively establish single-stage, diffusion-controlled multilayer corona growth from step-wise,

sequential growth in response to changing *P-T* conditions or component fluxes. In these cases, tectonic context and structural data might provide independent constraints favouring one model over the other. Ultimately, clarification is best attained by modelling the spatial arrangement of textures in a series of chemical potential phase diagrams, which allow the full range of possible textural configurations given different formation mechanisms to be evaluated (White & Powell, 2011; Štípská et al.,

5   2010; Baldwin et al., 2015).

4.3 Reactant compositions

The compositions of local reactants principally determine the effective bulk composition of the corona, with a minor degree of open-system communication with matrix beyond the immediate reactants. The most obvious manifestation of local compositional control on corona configuration is demonstrated by the three main types of coronas observed in mafic rocks,

10 where metasomatic exchange with the enclosing rock is minimal and the corona bulk composition is principally determined by the reactants. Local corona bulk compositions comprising orthopyroxene, clinopyroxene, plagioclase and garnet form after olivine and plagioclase (*Ol*│Opx│Cpx│Pl│Grt│*Pl* – Fig. 2, 3 and 5). More aluminous, hydrous corona bulk compositions after garnet and clinopyroxene with an externally-derived H$_2$O-rich fluid stabilise amphibole, plagioclase and orthopyroxene (*Grt*│Prg│Pl│Cpx/Opx│*Cpx* – Fig. 7c, d). Commonly, clinopyroxene reacts with plagioclase to yield

15 clinopyroxene (with or without orthopyroxene), quartz and garnet coronas (*Cpx*│Cpx/Opx│Qtz│Grt│*Pl* – Fig. 7e, f).

Markl et al. (1998) described coronas after fayalite and K-feldspar or plagioclase (*Fa*│Opx│Grt+Opx│*Pl/Kfs*), in which the layer thicknesses, product proportions and their compositions vary systematically depending on whether plagioclase or K-feldspar is the reactant. Carlson and Johnson (1991) described a corona after garnet and quartz in a metagabbro from the Llano Uplift in Texas comprising the layer sequence *Grt*│Pl+Mgt│Opx+Aug│*Qtz*. In metapelites, coronas after garnet and

20 quartz typically yield a coronal assemblage of *Grt*│Crd+Opx│±Pl│Opx│*Qtz* (Hollis et al., 2006 – Fig 8b). The presence of augite, plagioclase and magnetite in the metagabbro may be attributed to significantly more calcic garnet (~8 wt% CaO) with a higher X_{Fe} than typical pelitic garnets. Van Lamoen (1979) and Nishiyama (1983) reported coronas after olivine and plagioclase in metamafic rocks and conclusively demonstrated a correlation between the compositions of reactant olivine and product orthopyroxene.

25 Sectoral development in complex coronas is perhaps the most obvious manifestation of reactant compositional control on corona mineralogy and morphology. Kelsey et al. (2003b) described sectoral development of coronas around garnet in pelitic granulites from the Mather paragneiss in the Rauer Group, Antarctica (Fig. 8c). In these granulites, garnet is enclosed by a complex corona that comprises *Grt*│Crd+Opx symplectite│Opx│*Qtz* where garnet was initially adjacent to quartz and *Grt*│Crd+Opx symplectite│Pl│*Bt*, where initially adjacent to biotite. These corona sectors appear to define unique, highly

30 localised, effective bulk compositions. The sharp changes in mineral proportions between sectors attests to the limited degree of chemical communication between the Grt-Bt and Grt-Qtz compositional domains. Bruno et al. (2001) described coronas

after biotite and quartz or feldspar, in which corona mineralogy varies around a single biotite grain from $Bt│Grt│Qtz$ where biotite abuts quartz, to $Bt│Grt│Grt+Qtz│Phg+Qtz│Kfs$ where biotite is adjacent to K-feldspar and $Bt│Grt│Grt+Jd│Pl$ where plagioclase encloses biotite (Fig. 8d). Štípská et al. (2010) noted complex radial and sectoral heterogeneity in coronas after kyanite (Fig. 8h). Where kyanite is enclosed by plagioclase-K-feldspar-quartz matrix, it is replaced by a reasonably

5 uniform corona comprising $Ky│Pl+Sp±Crn$ symplectite $│Pl│Matrix$. The monomineralic plagioclase layer is strongly zoned with respect to anorthite content, grading from $X_{An}=0.45$ to 0.20 adjacent to the matrix. Locally, where kyanite abuts garnet from the peak assemblage, the plagioclase-spinel symplectite is absent and a thin Ca-poor garnet monomineralic layer is rather developed, which is in turn enclosed by unzoned monomineralic plagioclase. Štípská et al. (2010) ascribed the antipathetic occurrence of the garnet corona layer and the spinel+plagioclase symplectite to higher FeO and MgO chemical

10 potentials in the equilibration volume encompassing both garnet and kyanite as a reactant, which stabilised garnet in the calculated product phase equilibria.

4.4 Diffusion kinetics

The spatial array of corona product bands and the presence or absence of associated symplectite is a function of ~~diffusion kinetics, i.e., relative intergranular diffusivities of major system components.~~ Typically, Al and Si are relatively immobile

15 compared to more rapidly diffusing components such as Fe, Mg and, to a lesser extent, Ca (e.g., Johnson and Carlson, 1990; Carlson and Johnson, 1991; Ashworth and Birdi, 1990; Ashworth et al., 1992; Ashworth and Sheplev, 1997). In natural coronas that have formed in a single-stage, steady-state, diffusion-controlled scenario, typically limited Al diffusion manifests as both modal and phase compositional zonation in the corona, i.e., Al-rich minerals occur in layers closest to the aluminous reactant and, within these layers, the corona minerals exhibit asymmetric zonation in compositional profiles, e.g.,

20 y(Opx) increases toward the Al-rich reactant. Since Fe and Mg typically diffuse more rapidly than Al, ferromagnesian minerals tend to segregate into layers farthest from the aluminous reactant. X_{Fe} varies across the corona depending on relative intergranular diffusivities of Fe and Mg. Coronas after sapphirine and quartz in metapelites (Ellis et al., 1980 – Fig. 8e) and between sillimanite and orthopyroxene (Kriegsman et al., 1999; Appendix 2) demonstrate spatial segregation of aluminous corona layers (sillimanite and sapphirine, respectively) from more Fe- and Mg-rich corona products (orthopyroxene and

25 cordierite, respectively). Coronas after garnet and clinopyroxene in more mafic bulk compositions segregate into pargasite adjacent to garnet and orthopyroxene+plagioclase adjacent to clinopyroxene (Baldwin et al., 2004 – Fig. 7d).

~~Kinetically-constrained reaction rates arise most commonly on the retrograde *P-T* path (Appendix 2) in melt-depleted, restitic bulk rock compositions. In metapelites, coronal reaction textures are commonly attributed to isothermal decompression following peak conditions on a clockwise *P-T* path (e.g., coronas after garnet and quartz; Kelsey et al., 2003b~~

30 ~~– Fig. 8c) or to isobaric cooling (e.g., coronas after sapphirine and quartz; Grew, 1980 – Fig. 8e). White et al. (2002), however, urge caution in inferring large amounts of decompression and cooling along the retrograde path to produce corona textures; phase equilibria modelling of spinel-bearing symplectites after garnet from an Fe-rich pelitic granulite in the~~

~~Musgrave Block, Australia (Fig. 8f), suggested to them that coronas might develop on any number of retrograde *P-T* path trajectories through a high-variance field in which the mode of garnet is decreasing while that of the corona products is increasing. Large amounts of decompression are, thus, not required to produce coronas and symplectites after garnet and estimates of decompression from other terranes (e.g., Harley, 1989) may well have been overestimated.~~

5 Coronas developed on the prograde path (Appendix 1) are far less common than coronas that form after peak phases during retrogression (Appendix 2), owing largely to more prolonged reaction duration; the presence of a melt or fluid and, hence, greater length-scales of diffusion; and associated deformation on the prograde path. Thus, the kinetically-constrained conditions on the prograde path suitable for corona growth occur in unique tectonic circumstances where deformation is absent (e.g., White and Clarke, 1997 – Fig. 7e), at low aH$_2$O in mafic rocks (Ashworth et al., 1998 – Fig. 7f; Johnson and

10 Carlson 1990 – Fig. 2) or in melt-depleted pelitic restites, or where the rate of change of pressure and temperature occurs anomalously quickly such that diffusion rates are exceeded. Typically, the latter scenario arises in contact aureoles characterised by rapid heating and cooling (Johnson et al., 2004 – Fig. 8g; Mcfarlane et al., 2003; Ings and Owen, 2002; Barboza and Bergantz, 2000; Wheeler et al., 2004; Daczko et al., 2002; Dasgupta et al., 1997; Joesten and Fisher, 1988), but it can also occur in shock-heated rocks within large impact structures (Gibson, 2002; Ogilvie, 2010).

15 **4.5 Deformation and strain**

High strain intensities have been shown to enhance equilibration (Holyoke and Tullis, 2006). White and Clarke (1997) described coronas developed after orthopyroxene and plagioclase in a dolerite adjacent to a shear zone in the Western Musgrave Block, Australia (Fig. 7e). Towards the shear zone, coronas diminish in complexity until complete equilibration and recrystallisation is attained in the highest strain domains within the shear zone. Koons et al. (1987) documented similar

20 findings in a quartz diorite from the Sesia Zone, Western Alps, whilst Smit et al. (2001) described enhanced replacement of garnet by, and deformation of, orthopyroxene+cordierite symplectite approaching bounding shears zones in the Limpopo Belt, South Africa. With increasing deformation, equilibrium domains progressively approach that of the bulk rock composition without any discernable change in pressure and temperature. White and Clarke (1997) attributed this enhanced equilibration in high-strain domains to a combination of reduction in grain size with attendant increase in intergranular area,

25 accelerated intracrystalline diffusion and nucleation, and increased permeability and aH$_2$O.

5 Conditions of corona formation

In general, thermobarometric estimates for the average *P-T* conditions of corona formation in mafic and pelitic rocks are above the wet solidus for their respective bulk rock compositions (Fig. 9). The few exceptions plotting below the solidus may be attributed to retrograde compositional resetting with cooling. Fig. 9 is consistent with corona formation at granulite

30 facies temperatures in rocks that have an intrinsically anhydrous bulk rock composition (e.g. mafic granulites) or have undergone a degree of melt loss. Under these conditions, intergranular diffusion limits reaction rate and extent of

equilibration, especially when melt is absent in coarse-grained assemblages. Retrograde corona development is likely constrained to the portion of the *P-T* path immediately following peak T. Since most melt is lost at or near peak conditions (White and Powell, 2002), only a fraction of melt is retained in the restitic post-peak assemblage. Reduced melt volumes limit length-scales of diffusion during cooling to the extent that diffusion-controlled corona growth occurs. On the prograde

5   path, the low/absent melt volumes required for kinetically-constrained corona growth are only commonly realised in mafic rocks, owing to their intrinsic anhydrous bulk composition, and in dry, restitic pelitic compositions that have lost melt in an earlier metamorphic event. White and Powell (2011) distinguish two types of coronas formed either on the prograde or retrograde paths, namely, progressive or non-progressive. Progressive coronas develop on the same *P-T* path as the assemblage that they replace, in response to a smooth change in *P-T* conditions from those that produced the peak

10 assemblage (e.g., Johnson et al., 2004; Hollis et al., 2006; Kelsey et al., 2003b). Non-progressive coronas develop in a separate *P-T* event to those that generate the peak assemblage (e.g., Johnson and Carlson, 1990; Gibson, 2002; McFarlane et al., 2003).

6 Corona microstructure

Corona microstructure in prograde and retrograde coronas for which data is available is summarized in Figs. 10 and 11. The

15 average maximum corona layer thickness in mafic prograde coronas is 475 μm (range: 70-1000 μm, n = 19) and average maximum vermicule size is 118 μm (range: 50-300 μm, n = 19). Pelitic prograde coronas are characterized by an average maximum corona thickness of 496 μm (range: 75-1500 μm; n = 13) and an average maximum vermicule size of 115 μm (range: 10-300 μm, n = 13). Thus, mafic and pelitic prograde coronas do not differ significantly with respect to maximum corona layer thickness and vermicule size. However, pelitic prograde coronas developed in contact metamorphic aureoles

20 appear to exhibit greater maximum corona layer thicknesses (>500 μm) compared to regional pelitic prograde coronas (Fig. 10a).

Most retrograde coronas described in the literature occur in pelitic bulk compositions (Appendix 2; Figure 11). Pelitic retrograde coronas are characterized by an average maximum corona thickness of 571 μm (range: 100-3000 μm; n = 28) and an average maximum vermicule size of 147 μm (range: 20-500 μm, n = 28). The average maximum corona layer thickness

25 in mafic retrograde coronas is 262 μm (range: 80-500 μm, n = 5) and average maximum vermicule size is 27 μm (range: 10-40 μm, n = 5). Whilst retrograde pelitic coronas do not differ significantly from prograde pelitic coronas in terms of width and vermicule size, retrograde mafic coronas are distinctly narrower and show significantly reduced vermicule size relative to prograde mafic coronas (Fig. 11) The latter most likely reflects greater length-scales of melt-enhanced diffusion along the prograde path. A similar relative paucity of melt may explain the difference in corona thickness and vermicule size in

30 retrograde mafic coronas compared to retrograde pelitic coronas.

7 Internal compositional zonation in coronas

Complex compositional zonation is commonly observed in coronas (Fig. 12). Fully equilibrated coronas, where no compositional zonation or chemical potential gradients exist, are rare. In the population of coronas studied, only 30% were fully equilibrated, of which 60% were in pelitic bulk compositions. Commonly, coronas exhibit asymmetric zonation across

5   the band as a whole, reflecting variable length-scales of diffusion for major components during single-stage, steady-state growth (e.g., Ashworth et al., 1998 - A98; Johnson et al., 2004 - J04, Figure 12). Less commonly, radial zonation occurs within a product layer or vermicule from the band centre/vermicule core to the rim, indicative of sequential corona growth (e.g., Zulbati et al., 2007 - ZH07, Fig. 12). The maximum magnitude of zonation in X_{Mg} of orthopyroxene across a corona band in the coronas reviewed is 0.08 (Kriegsman et al., 1999 - K99; Osanai et al., 2004 - O04; Fig. 12) and 0.07 in cordierite

10   (Baker et al., 1987 - BKS87; Fig. 12). Unfortunately, Al content in orthopyroxene is expressed as y(Opx), Al^{IV} and Al wt% in the literature commonly without accompanying raw analyses, so that these values cannot be recomputed to a single formulation of Al in orthopyroxene to aid comparison. Maximum asymmetric zonation magnitude with respect to y(Opx) is 0.08 in Hollis et al. (2006 - H06; Fig. 12); 0.13 with respect to Al^{IV} (a.p.f.u.) (Brandt et al., 2003 - BKO03; Fig. 12) and 0.05 with respect to recalculated molecular proportion (Hisada and Miyano, (1996) - H96; Fig. 12). Maximum magnitude of

15   zonation in garnet is 0.22 for X_{Grs} (White and Clarke, 1997 - WC97; Fig. 12), 0.18 for X_{Alm} (Indares, 1993 - I93; Fig. 12) and 0.17 for X_{Prp} (Koons et al., 1987 - K87; Fig. 12). Maximum magnitude in plagioclase zonation (ΔX_{An}) is 0.42 (Baldwin et al., 2004 - B04; Fig. 12).

Product phase zonation makes the application of quantitative thermobarometry exceptionally difficult. Asymmetric compositional zonation is consistent with steady-state, diffusion-controlled layer growth and, in this case, local equilibria

20   between mineral pairs in corona layers do not reflect discrete *P-T* conditions but, rather, compositional partitioning of the corona domain during steady-state growth at constant *P* and *T*. Symmetric, radial zoning of phases with respect to grain boundaries is more consistent with a sequential corona formation model, where initially corona layers may develop by steady-state diffusion at (P_1,T_1), equilibrate given sufficient time and then, with subsequent change in *P* and *T,* partially re-equilibrate under new *P-T* conditions (P_2, T_2) that are reflected in the rim compositions (e.g., White and Clarke, 1997).

25   In some instances, corona product phases in local equilibrium adjacent to a reactant possess low enough variance to apply a conventional thermobarometer. For example, Baldwin et al. (2004) obtained *P-T* conditions of corona formation from Grt-Opx-Pl-Qtz equilibria using garnet rim and orthopyroxene-plagioclase symplectite compositions in direct contact. Some authors have applied conventional thermobarometers to spatially segregated phases in a corona that are not in direct contact (e.g., Perchuk et al., 2002; Brandt et al., 2003). This approach is only valid if there is no variation in phase composition

30   across the corona band and chemical potentials gradients do not exist.

Ashworth et al. (1998) derived a non-equilibrium extension to conventional thermobarometry based on open-system, steady-state diffusion modelling of coronas that has been successfully employed to estimate *P-T* conditions of formation of asymmetrically-zoned coronas (Ashworth et al., 2001). Unfortunately, non-equilibrium thermobarometry, like conventional thermobarometry, is very sensitive to uncertainties in compositional data and prone to underestimating peak temperatures of

5   formation, because of retrograde resetting upon cooling. The preferred thermobarometric technique for coronas entails phase equilibria modelling in THERMOCALC (e.g., Baldwin et al., 2015), where modes and phase compositions are used to jointly constrain a field of equilibration in *P-T-X* space. THERMOCALC allows the modelling of corona textures in chemical potential space (White et al., 2008; White and Powell, 2011; Štípská et al., 2010 and Baldwin et al., 2015) facilitating direct comparison of the observed phase zonation and spatial array of layers across a corona in which chemical

10   potential gradients prevail with predicted compositions at a range of temperatures and pressures.

8 Modelling of coronas

Diffusion modeling of metamorphic reactions began in earnest with the foundational work of Thompson (1959) and Korzhinskii (1959), who demonstrated that infinitesimally small regions of rock can attain local equilibrium in the presence of chemical potential gradients for all or some components. This meant that even if the system is in disequilibrium as a

15   whole, with gradients in chemical potentials of components in the intergranular medium, it is nevertheless possible to relate the mineral assemblage at any point to the chemical potentials at that point. Korzhinskii (1959) devised a graphical method for plotting a saturation surface in chemical potential space that allowed determination of relative chemical potential differences across a series of layers (Figure 1). This method facilitated an understanding of how layer sequences would evolve as components diffuse down chemical potential gradients. The limitation of Korzhinskii's technique is that many

20   diffusion paths from one reactant to another are possible in the chemical potential diagram, such that more than one possible layer sequence could evolve for a particular *P-T* condition (Nishiyama, 1983). The advances in thermodynamic formulations of phases required to model these relationships would only be developed by workers in later decades (Powell & Holland, 1988; Powell & Holland, 1990; Holland & Powell, 1998; Powell et al., 1998; Holland & Powell, 2003; Powell et al., 2005; Holland & Powell 2011; White et al., 2014), and even then only readily applied to coronas using the appropriate activity-

25   composition relationships through pioneering studies by White et al. (2008); Štípská et al. (2010) and Baldwin et al. (2015). In the interim, workers modelled coronas through a quantitative physico-chemical modelling approach, in which component fluxes and chemical potential gradients required to reproduce observed corona layers configurations were derived assuming reaction was driven and governed by minimisation of entropy.

8.1 Quantitative physical modelling of coronas

30   The quantitative physical modelling of coronas is premised on the fact that in layered reaction products, mineral layers grow by reaction at their contacts and the stoichiometries of the layer contact reactions are determined by the relative diffusion fluxes of components within the layer. Component fluxes and chemical potential differences across each layer attain steady-

state values as a function of the rate of production and consumption of phases in the layer (Fisher, 1975). Joesten (1977) combined the approaches of Fisher (1975) and Korzhinskii (1959) into a hybrid methodology that allowed the prediction of a unique sequence of mineral layers produced by steady-state diffusion for a given choice of phenomenological coefficients in an isochemical system. Joesten's model is based on three fundamental assumptions: first, diffusing components are in local

5   equilibrium with contiguous minerals at every point in a corona, despite the fact that the corona as a whole is in disequilibrium; second, component fluxes and chemical potential gradients remain constant at each point in the corona in a steady-state throughout its evolution; and third, all components are considered to be conserved within the reaction band, i.e., there is no communication with a system beyond the boundaries of the reaction bands (the system is closed).

Joesten's model required the simultaneous solution of three sets of equations independently relating component fluxes to

10   chemical potential gradients in a layer, chemical potential gradients to each other in the presence of a mineral with a particular composition, and the flux change between layers to reaction coefficients at layer boundaries (Ashworth and Sheplev, 1997). It is possible to evaluate the stability of a multilayer reaction band for a postulated set of intergranular diffusion coefficients if the compositions of the phases in each band are known. The model predicts the relative widths of layers in the reaction band, modal proportions of phases within each layer, component fluxes across layers and reaction

15   stoichiometry at layer boundaries.

Early attempts to model corona textures using Joesten's formalism focussed on corona reaction bands formed between olivine and plagioclase in metagabbros (e.g., Nishiyama, 1983; Joesten, 1986; Grant, 1988). This early work was hindered by the closed system constraint in Joesten's model. For example, Grant (1988) was unable to produce enough Ca from the observed reactant plagioclase to accommodate all the Ca in the corona reaction band. Furthermore, the failure of Joesten's

20   model to account for hydrous corona products, such as hornblende, from anhydrous plagioclase and olivine reactants, led workers to embrace an open-system, metasomatic, modification to Joesten's model. An open-system modification was introduced by Johnson and Carlson (1990) and Ashworth and Birdi (1990). Material balance calculations allowed them to determine the external component fluxes across the outer boundaries of the corona, thereby accommodating open-system communication with the enclosing matrix. Johnson and Carlson (1990) and Carlson and Johnson (1991) introduced external

25   boundary flux equations to model open-system behaviour. Ashworth and Birdi (1990) treated metasomatic fluxes at corona boundaries as theoretical 'phases' with 'negative' compositions where components were lost from the system and 'positive' compositions where they entered into the corona system. The open system studies of Johnson and Carlson (1990) and Carlson and Johnson (1991) also indicated that corona growth may not occur as a 'single-stage, steady-state process', but rather through a number of 'transient states', reflecting gradual changes in the composition of the reactants and external

30   fluxes throughout corona evolution, thus manifesting as variable product assemblages (Figure 7a).

Open-system diffusion models for coronas had much more success in explaining corona development in a variety of different bulk compositions, from mafic rocks to metapelites, than the earlier isochemical models (Johnson and Carlson,

1990; Carlson and Johnson, 1991; Ashworth and Birdi, 1990; Ashworth et al., 1992; Ashworth, 1993; Ashworth and Sheplev, 1997; Ashworth et al., 1998). Ashworth (1993) noted that, although the overall extent of reaction was constrained by highly mobile components with large diffusive fluxes, the actual spatial arrangement of minerals in coronas appears to be strongly controlled by those components with lower diffusivities, particularly Al and Si. He noted that, in all cases, an Al-

5   rich layer (commonly symplectitic) was located adjacent to the most aluminous reactant, grading into an Al-poor layer adjacent to the less aluminous reactant, and both separated by a 'transitional' layer of intermediate contents of Al (Figure 13).

Ashworth and Birdi (1990) compared the Al/Si ratio in aluminous reactants and the adjacent symplectite for a number of coronas using an isocon diagram (Figure 14; Grant, 1986). The isocon plot suggested that total Al and Si (strictly $AlO_{3/2}$ and

10   SiO_2, since the components used are oxides ~~following Fisher, 1973~~) included within the phases in the symplectite appear to be 'inherited stoichiometrically' from the adjacent reactant. Any mismatch between Al/Si ratio of the reactant and individual phases comprising the symplectite is accommodated by proportional growth of symplectite phases in the appropriate ratio such that cumulatively the Al/Si ratio is retained. Ashworth and Birdi (1990) proposed that this was a consequence of low diffusivities of Al and Si relative to~~, inter alia,~~ Fe, Mg and Ca. According to them, any disagreement between the Al/Si ratio

15   of the symplectite and reactant implies open-system behaviour for these components. The endmember scenario involving near-complete open-system behaviour for Al and Si would, thus, be a monomineralic reaction band in which mismatch in Al/Si ratio is greatest. Mongkoltip and Ashworth (1983) ventured still further that the occurrence of two immobile diffusing components is a necessary condition for symplectite formation. This assertion agreed with the metasomatic equilibrium theory of Korzhinskii (1965), which states that any divariant equilibrium assemblage of n phases contains at least n inert or

20   immobile components. Assessing open- or closed-system behaviour for Al and Si is critical in deciding which assumptions are realistic when determining the overall reaction. If Al and Si are preserved in the symplectite, then closure to Al and Si can be used to constrain the system such that it is not underdetermined. If this assumption is not valid, constant volume may have to be assumed (Carlson and Johnson, 1991).

The first thermodynamic treatment of conservation of volume during diffusion metasomatism was undertaken by Carmichael

25   (1987). Carmichael challenged the assumption that pressure remains constant during irreversible diffusion metasomatism. During reaction, there is a tendency for the boundary between two juxtaposed reactants to be displaced perpendicular to the interface between the reactants at a magnitude corresponding to the change of volume of solid phases of the reaction. If there is any mechanical resistance to this displacement, constant volume replacement is approached. Carmichael (1987) was able to model a field of nonhydrostatic stress induced by migration of the boundary between reactants. The stress field is oriented

30   in a manner which opposes the displacement and strain accompanying the migration of the boundary. The stress field may be dissipated by either rock deformation or secondary mass transfer out of the reacting volume. According to Carmichael's model, the secondary mass transfer may be so efficient as to eliminate the induced stress caused by boundary migration, such

that the original interface between reactants remains undisplaced. This realisation allows reasonable approximations to be made for the original boundary between reactants (and the relative proportions of reactants involved in reaction) such that an overall reaction may be derived.

In this context, the spacing of lamellae or vermicules in symplectites reflects a balance between diffusive energy dissipation and grain boundary energy. Ashworth and Chambers (2000) derived a theory quantifying this relationship employing both non-equilibrium thermodynamics and the principle of maximum rate of energy dissipation. Accordingly, the spacing of lamellae in a symplectite for a particular reaction is a function of the reaction rate (i.e., reaction front velocity), diffusion coefficient of the slowest-diffusing components and the width of the reaction front:

$$\lambda = \sqrt[3]{\frac{L\delta}{v}}$$

λ = lamellae spacing; L = Onsager ~~diffusion~~ coefficient

δ = reaction front width; v = reaction rate

The finest symplectitic intergrowths (closest lamellae spacing) are predicted to occur when reaction rates greatly exceed diffusion coefficients for the slowest-diffusing species for a particular reaction front width.

Despite advances in diffusion metasomatic modelling of coronas in the early 1990's, success was still limited in that commonly more than one stable layer sequence was computable for the same inputs. Sheplev et al. (1991, 1992a, b) presented a criterion to determine which non-unique solution is more thermodynamically stable compared to others and is, thus, the correct solution. The criterion was formalized by Ashworth and Sheplev (1997), and extended so as to obtain a measure of the affinity of reaction or, rather, departure from equilibrium, preserved in the corona. A final refinement to the open-system diffusion model for coronas was derived by Ashworth et al. (2001), in which ratios of the affinity of independent endmember reactions modelled for a corona are compared to ratios calculated from an internally-consistent thermodynamic database (Holland and Powell, 1998). The pressure and temperature where the ratio of model endmember reaction affinities and real endmember reaction affinities approach the same value is considered to represent the closure pressure and temperature below which the corona remained inert to reaction. This allowed quantitative estimates of pressure and temperature of formation of minerals in disequilibrium to be made.

8.2 Calculated phase equilibria modelling

A limitation of the quantitative physical modelling of coronas outlined above is that solid solutions and the gradational shifts in phase composition within a band cannot practically be accounted for in the modelling (White and Powell, 2011; Baldwin

et al. 2015). In the last decade, advances in phase equilibria modelling have allowed geologically realistic corona compositional systems to be modelled in *P-T-X* (Johnson et al., 2004) and chemical potential space (White et al., 2008; Štípská et al., 2010; White & Powell, 2011; Baldwin et al., 2015). It is possible to predictively model corona evolution with changing effective bulk composition through progressive metasomatic exchange of components with the external matrix in a
5   rock and/or partitioning of the corona effective bulk composition with reduced length-scales of component diffusion on cooling (e.g., Johnson et al., 2004; White et al., 2008; Štípská et al., 2010; Baldwin et al., 2015).

One of the most robust and elegant applications of chemical potentials in constraining corona textural and compositional evolution in *P-T-X* space is that undertaken by Štípská et al (2010). These workers modelled coronas developed after kyanite in a quartzofeldspathic gneiss from the Bohemian Massif (Figure 8h). Phase equilibria modelling entailed an initial estimate
10   of overall *P* and *T* conditions prevailing using a conventional *P-T* pseudosection in NCKFMASHTO (Štípská et al., 2010). For the purpose of phase equilibria modelling in chemical potential space, it is necessary to reduce the number of components treated, based on assumptions considering their inferred relative mobility. Štípská et al., (2010) ranked components in the corona according to a hierarchy of mobility or relative diffusivities, i.e., slowest diffusing components are considered effectively immobile (i.e., chemical potential gradients are static and cannot change during reaction); other
15   components are considered mobile (their chemical potential gradients vary on the scale of the corona); and some components are treated as completely mobile (their chemical potentials do not vary across the corona and are superimposed by the matrix). Accordingly, Štípská et al., (2010) were able to reduce the model compositional system to NCKFMAS.

Prior to their consideration of the ferromagnesian minerals in the corona, Štípská et al. (2010) modelled the monomineralic plagioclase moat in NCKAS, with the further assumption that K_2O is completely mobile and Al_2O_3 is immobile with static
20   potentials, i.e., it is treated as an extensive variable, in terms of phase composition. The chemical potentials for the matrix edge of the corona correspond to those for the equilibrated peak assemblage and the corona plagioclase composition in local equilibrium with matrix (i.e., An_{20}) (Fig. 15a). The chemical potentials for the metastable kyanite corona contact were derived by modifying $\mu(Na_2O)$ at the matrix contact until the kyanite-plagioclase boundary with An_{45} appears on the phase diagram (Fig. 15a). In Fig. 15a, the chemical potential relations at the kyanite and matrix boundary are overlain in $\mu(CaO)$-
25   $\mu(SiO_2)$ space and local equilibrium potentials indicated. Since the values of $\mu(Na_2O)$, $\mu(CaO)$ and $\mu(SiO_2)$ differ between the two equilibria, a chemical potential gradient is established and is represented by the vector in Fig. 15a. For equilibrium to be attained throughout the corona, chemical potentials must be equalised everywhere by diffusion. If diffusion is kinetically constrained, these chemical potential gradients persist as stranded gradients in chemical potential (Baldwin et al., 2015).

Stipska et al. (2010) modelled the presence or absence of a garnet layer in the corona by superimposing $\mu(FeO)$ and $\mu(MgO)$
30   variations on the vector in $\mu(Na_2O)$-$\mu(CaO)$-$\mu(SiO_2)$ space obtained in Fig. 15b. The authors calculated $\mu(FeO)$- $\mu(MgO)$ diagrams for the matrix boundary, kyanite boundary and midway between the them with respective $\mu(Na_2O)$-$\mu(CaO)$-$\mu(SiO_2)$ dictated by the vector constrained in NCKAS space (Figure 15a). The observed composition of garnet ($X_{Fe} = 0.70$),

defines a corresponding vector in μ(FeO) and μ(MgO) space (Figure 15b). Stipska et al. (2010) manually constructed a phase diagram by combining the phase relations along the $X_{Fe} = 0.70$ vector in μ(FeO) and μ(MgO) space with those corresponding in μ(Na$_2$O)-μ(CaO)-μ(SiO$_2$) space (Fig. 15c). Two observed chemical potential paths were proposed to account for garnet-present and garnet-absent coronas that reproduced the known spatial array and composition of phases.

5   They suggest that the chemical potential path required to produce garnet requires the μ(FeO) and μ(MgO) potentials to be boosted relative to those in local equilibrium with the matrix. This is consistent with the spatial association of original matrix garnet in the corona, such that the μ(FeO) and μ(MgO) potentials are locally augmented, thereby stabilising a garnet layer in the coronas in the local equilibrium with kyanite (Štípská et al., 2010).

Modelling of the development of the plagioclase-spinel symplectite required that SiO$_2$ also be treated as immobile (Štípská et
10   al., 2010). Constrained SiO$_2$ diffusion from the matrix toward kyanite across the plagioclase moat induced a silica-deficient effective local bulk composition at the plagioclase-kyanite boundary, thus, lowering the local SiO$_2$ chemical potential sufficiently to stabilise spinel (assuming corundum was unable to nucleate). As a consequence, both SiO$_2$ and Al$_2$O$_3$ chemical potentials are treated as quasi-stationary, i.e., they are modelled as the coupled extensive composition variables. As a consequence, phase fields in mu-mu space are labelled with Al$_2$O$_3$-SiO$_2$ bar compatibility diagrams. Štípská et al. (2010)
15   proceeded to model the requisite chemical potentials for the symplectite stability initially in μ(Na$_2$O)-μ(CaO)-μ(SiO$_2$) space. They derived a vector in chemical potential space between the symplectite contact with the plagioclase moat and the kyanite boundary (Figure 15d) that accounted for the plagioclase composition within the symplectite. However, the restricted stability limits of spinel in mu-mu space at the modelled conditions of post-peak conditions led Štípská et al. (2010) to infer the spinel-bearing symplectites must have formed during subsequent decompression after plagioclase moat formation, as the
20   spinel stability field is far broader at lower pressures for the same potentials.

Similarly Baldwin et al. (2015) modelled spinel-plagioclase, sapphirine-plagioclase and corundum-plagioclase symplectites after kyanite in a quartzofeldspathic granulite gneiss from the Athabasca granulite terrane, Snowbird tectonic zone, Canada. These workers, like Štípská et al. (2010), deduced that the spinel-plagioclase symplectites must be metastable with respect to the corundum-bearing alternative. Assuming corundum was unable to nucleate, they were able to account for spatial
25   relationships and compositions observed in the symplectites over a wide range of P-T conditions and plagioclase compositions. Crucially they were able to deduce that, without the application of chemical potential phase diagrams suggesting otherwise, such reaction textures may occur over a wide range of P-T conditions and extreme caution must be exercised in inferring P-T conditions of retrograde metamorphism from them.

Štípská et al. (2010) and Baldwin et al. (2015) conclusively demonstrate that the use of chemical potentials is imperative and
30   unavoidable when investigating coronas. Previous workers (Johnson et al., 2004; Tajčmanová et al., 2007; Ogilvie, 2010) have attempted to model corona textures without the chemical potential phase diagrams. These authors invoked an equilibrium volume comprising the corona, with or without a matrix contribution, which they assumed to be effectively

closed system during textural development. Accordingly, corona growth involved a redistribution of chemical components within the limits of the equilibrium volume. This approach might account for some of the phases within the corona, but fails to account for the non-linear exchange of components both within local equilibria across the corona but also external metasomatic exchange with the enclosing matrix during corona evolution. Tajčmanová et al (2007) tried to circumvent this

5   problem by constructing a *T-X* section to model the compositional partitioning, owing to variable diffusion of components, across the corona, and predicted phases. Similarly, Ogilvie (2010) attempted to model shifts in corona phase compositions and modes through the inferred exchange of components between the corona effective bulk compositions and the external matrix through a *T-X* section involving pure reactants on one axis and pure matrix as the other axis. The fundamental problem with both these approaches, as noted by White & Powell (2011), is that at best, it is only possible to account for

10 observed assemblages in a qualitative generalised sense. This is because the high variance of the phase fields from the *T-X* section or *P-T* pseudosection predicts stable phases should be present in the coronas that are not actually observed. This can only be treated by considering some components as mobile, and removing them from the bulk composition utilised to model the corona. Crucially, the manner in which the chemical potentials evolve through *P-T* space involves non-linear changes in chemical potentials and local effective bulk compositions. Since *P-T* pseudosections are constrained at a static bulk

15 composition and a *T-X* section can only model linear changes in bulk composition, by their nature they are not flexible enough to allow modelling of the intricacies of corona development either owing to variable external component flux into the corona (for example, by melt ingress or loss) or variable multi-component length-scales of diffusion.

9 Discussion

Evidence of partial equilibrium, preserved in coronas, allows us to examine fundamental processes governing reaction

20 mechanism, rates and extents of equilibration in metamorphic (and, more rarely, igneous) rocks. Mechanisms of corona formation have been reviewed, i.e., *continuous*, single-stage, steady-state, diffusion-controlled vs. *non-continuous*, sequential development. A comprehensive review of prograde and retrograde coronas for mafic and pelitic bulk rock compositions from both regional and contact aureole terranes reveals that major controls on corona mineralogy include *P*, *T* and aH$_2$O during formation, mechanism of formation, reactant bulk compositions and extent of metasomatic exchange with the

25 surrounding rock, relative diffusion rates for major components, and associated deformation and strain. In general, corona formation occurs under granulite facies conditions, in anhydrous/restitic, melt-depleted bulk rock compositions (Fig. 9). With respect to corona microstructure, prograde coronas in pelitic rocks developed in contact metamorphic aureoles exhibit greater maximum corona thickness than those in regional coronas (Figure 11a). Mafic and pelitic prograde coronas do not differ significantly with respect to maximum corona layer thickness and vermicule size, however, corona thickness and

30 maximum vermicule size in retrograde mafic coronas are significantly smaller than both retrograde pelitic coronas and prograde mafic coronas, which likely attests to the role of melt in enhancing length-scales of diffusion during corona formation (retrograde mafic rocks are more likely to be melt-poor and anhydrous). Increased maximum layer thickness and vermicule size in prograde mafic coronas compared to retrograde mafic coronas (Fig. 11) may reflect greater length-scales of

diffusion in potentially more melt-rich bulk compositions with protracted reaction along the prograde path. Prograde pelitic coronas do not differ significantly from retrograde pelitic coronas with respect to microstructure (Fig. 11), owing to the intrinsically more hydrous pelitic bulk compositions and capacity to generate diffusion-enhancing melt during decompression.

5   High-variance local equilibria in a corona and disequilibrium across the corona as a whole preclude the application of conventional thermobarometry when determining *P-T* conditions of corona formation. Although tempting, the asymmetric zonation in phase composition across a corona, indicative of single-stage, steady-state, diffusion controlled formation, should not be interpreted as a record of discrete *P-T* conditions during successive layer growth along the *P-T* path. Rather, the local equilibria between mineral pairs in corona layers reflect compositional partitioning of the corona domain during steady-state

10   growth at constant *P* and *T*. A non-equilibrium extension of conventional thermobarometry derived by Ashworth et al. (2001) should be used with phase equilibria modelling in THERMOCALC to constrain *P-T* evolution of coronas (e.g., Ogilvie 2010).

Through the application of equilibrium thermodynamics at an appropriate scale (i.e., that of local equilibrium – Korzhinksi, 1959; Thompson 1959), corona evolution can be modelled either through quantitative physico-chemical diffusion modelling

15   (Johnson and Carlson, 1990; Carlson and Johnson, 1991; Ashworth and Birdi, 1990; Ashworth et al., 1992; Ashworth, 1993; Ashworth and Sheplev, 1997; Ashworth et al., 1998) or calculated phase equilibria involving chemical potentials (White et al., 2008; Štípská et al., 2010; White & Powell, 2011; Baldwin et al., 2015). While the former allows quantification of reaction affinity and chemical potential gradients across coronas bands, it is unable to practically accommodate variation in phase composition within a band. Moreover, it assumes that corona layer configuration formed during one, continuous,

20   single-stage, diffusion-controlled process, i.e., component flux between local equilibria across all bands in the corona was controlled by chemical potential gradients at that scale. In contrast, forward modelling utilising calculated chemical potential gradients to account for corona phase compositions and layer array, assumes nothing about the sequence in which the layers form and, since chemical potential gradients prevailing are constrained by observed phase compositional variation within a layer, it allows far more nuanced yet robust understanding of corona evolution and the implications for the path followed by

25   a rock in *P-T-X* space.

10 Acknowledgments

Funding from the National Research Foundation Scarce Skills Scholarship and Rated Researcher Programmes is gratefully acknowledged.

References

Abart, R., Schmud, R., Harlov, D.E.: Metasomatic coronas around hornblendite xenoliths in granulite facies marble, Ivrea zone, N Italy, I: Constraints on component mobility, Contributions to Mineralogy and Petrology, 141, 473-493, 2001.

Álvarez-Valero, A. M., Cesare, B., Kriegsman, L.M.: Formation of spinel-cordierite-feldspar-glass coronas after garnet in
5   metapelitic xenoliths: reaction modelling and geodynamic implications, Journal of Metamorphic Geology, 25, 305-320, 2007.

Ashworth, J. R.: The role of magmatic reaction, diffusion, and annealing in the evolution of coronitic microstructure in troctolitic gabbro from Risor, Norway: a discussion, Mineralogical Magazine, 50, 469-473, 1986.

Ashworth, J. R.: Fluid-absent diffusion kinetics of Al inferred from retrograde metamorphic coronas, American
10   Mineralogist, 78, 331-337, 1993.

Ashworth, J. R., Birdi, J. J.: Diffusion modelling of coronae around olivine in an open system, Geochimica et Cosmochimica Acta, 54, 2389-2401, 1990.

Ashworth, J. R., Birdi, J. J., Emmett T. F.: A complex corona between olivine and plagioclase from the Jotun Nappe, Norway, and the diffusion modelling of multimineralic layers, Mineralogical Magazine, 56, 511-525,1992.

15 Ashworth, J. R., Chambers, A. D.: Symplectic reaction in olivine and the controls of intergrowth spacing in symplectites, Journal of Petrology, 41, 285-304, 2000.

Ashworth, J. R., Sheplev, V. S.: Diffusion modelling of metamorphic layered coronas with stability criterion and consideration of affinity, Geochimica et Cosmochimica Acta, 61, 3671-3689, 1997.

Ashworth, J. R., Sheplev, V. S., Bryxina, N. A., Kolobov, V. Y., Reverdetto, V. V.: Diffusion-controlled corona reaction
20 and over-stepping of equilibrium in a garnet granulite, Yenisey Ridge, Siberia, Journal of Metamorphic Geology, 16, 231-246, 1998.

Ashworth, J. R., Sheplev, V. S., Khlestov, V. V., Ananyev, A. A.: Geothermometry using minerals at non-equilibrium: a corona example European, Journal of Mineralogy, 13, 1153-1161, 2001.

Baker, J., Powell, R., Sandiford, M., Muhling, J.: Corona textures between kyanite, garnet and gedrite in gneisses from
25 Errabiddy, Western Australia, Journal of Metamorphic Geology, 5, 357-370, 1987.

Baldwin, J. A., Bowring, S. A., Williams, M. L., Williams, I. S.: Eclogites of the Snowbird tectonic zone petrological and U-Pb geochronological evidence for Paleoproterozoic high-pressure metamorphism in the western Canadian Shield, Contributions to Mineralogy and Petrology, 147, 528-548, 2004.

Baldwin, J. A., Powell, R., White, R. W., Štípská, P.: Using calculated chemical potential relationships to account for

5   replacement of kyanite by symplectite in high pressure granulites, Journal of Metamorphic Geology, 33, 311-330, 2015.

Barboza, S. A., Bergantz, G. W.: Metamorphism and Anatexis in the Mafic Complex Contact Aureole, Ivrea Zone, Northern Italy, Journal of Petrology, 41, 1307-1327, 2000.

Brady, J. B.: Metasomatic zones in metamorphic rocks, Geochimica et Cosmochimica Acta, 41, 113-125, 1977.

Brady, J. B.: Intergranular diffusion in metamorphic rocks, American Journal of Science, 283A, 181-200, 1983.

10   Brandt, S., Klemd, R., Okrusch, M.: Ultrahigh-Temperature Metamorphism and Multistage Evolution of Garnet-Orthopyroxene Granulites from the Proterozoic Epupa Complex, NW Namibia, Journal of Petrology, 44, 1121-1144, 2003.

Bruno, M., Compagnoni, R., Rubbo, M.: The ultra-high pressure coronitic and pseudomorphous reactions in a metagranodiorite from the Brossasco-Isasca Unit, Dora-Maira Massif, western Italian Alps: a petrographic study and equilibrium thermodynamic modelling, Journal of Metamorphic Geology, 19, 33-43, 2001.

15   Carlson, W. D.: Scales of disequilibrium and rates of equilibration during metamorphism, American Mineralogist, 87, 185-204, 2002.

Carlson, W. D., Johnson, C.D.: Coronal reaction textures in garnet amphibolites of the Llano Uplift, American Mineralogist, 76, 756-772, 1991.

Carmichael, D. M.: Induced stress and secondary mass transfer: thermodynamic basis for the tendency toward constant-

20   volume constraint in diffusion metasomatism, in: Chemical Transport in Metasomatic Processes, C 218, NATO Adv. Study Inst., Ser., 239-264, 1987.

Daczko, N. R., Stevenson, J. A., Clarke, G. L., Klepis, K. A.: Successive hydration and dehydration of high-P mafic granofels involving clinopyroxene-kyanite symplectites, Mt Daniel, Fiordland, New Zealand, Journal of Metamorphic Geology, 20, 669-682, 2002.

25   Dasgupta, S., Ehl, J., Raith, M. M., Sengupta, P., Sengupta, P.: Mid-crustal contact metamorphism around the Chimakurthy mafic-ultramafic complex, Eastern Ghats Belt, India, Contributions to Mineralogy and Petrology, 129, 182-197, 1997.

Droop, G. T. R.: Reaction history of garnet-sapphirine granulites and conditions of Archaean high-pressure granulite-facies metamorphism in the Central Limpopo Mobile Belt, Zimbabwe, Journal of Metamorphic Geology, 7, 383-403, 1989.

Ellis, D. J.: Osumilite-sapphirine-quartz granulites from Enderby Land, Antarctica: P-T conditions of metamorphism, implications for garnet-cordierite equilibria and the evolution of the deep crust, Contributions to Mineralogy and Petrology,
5   74, 201-210, 1980.

Fisher, G. W.: Non-equilibrium thermodynamics as a model for diffusion-controlled metamorphic processes, American Journal of Science, 273, 897-924, 1973.

Fisher, G. W.: The thermodynamics of diffusion-controlled metamorphic processes, in: Mass Transport Phenomena in Ceramics, Plenum Press, New York, 111-122, 1975.

10   Fisher, G. W.: Nonequilibrium thermodynamics in metamorphism, in: Thermodynamics in Geology, D. Reidel, 381-403 , 1977.

Foster, C. T.: Thermodynamic models of reactions involving garnet in a sillimanite/staurolite schist, Mineralogical Magazine, 50, 427-439, 1986.

Gibson, R. L.: Impact-induced melting in Archaean granulites in the Vredefort Dome, South Africa I.: Anatexis of
15   metapelitic granulites, Journal of Metamorphic Geology, 20, 57-70, 2002.

Grant, S. M.: Diffusion models for corona formation in metagabbros from the western Grenville Province, Canada, Contributions to Mineralogy and Petrology, 98, 49-63, 1988.

Grew, E. S.: Sapphirine+quartz association from Archaean rocks in Enderby Land, Antarctica, American Mineralogist, 65, 821-836, 1980.

20   Griffin, W. L.: Formation of eclogites and coronas in anorthosites, Bergen Arcs, Norway, Geological Society of America, Memoir, 135, 37-63, 1972.

Griffin, W. L., Heier, K. S.: Petrological implications of some corona structures, Lithos, 6, 315-335, 1973.

Harley, S. L.: The origins of granulites: a metamorphic perspective, Geological Magazine, 126, 215-247, 1989.

Hisada, K., Miyano, T.: Petrology and microthermometry of aluminous rocks in the Botswanan Limpopo Central Zone:
25   evidence for isothermal decompression and isobaric cooling, Journal of Metamorphic Geology, 14, 183-197, 1996.

Holland, T. J. B., Powell, R.: An internally consistent thermodynamic data set for phases of petrological interest, Journal of Metamorphic Geology, 16, 309-343, 1998.

Holland, T. J. B., Powell, R.: Activity-composition relations for phases in petrological calculations: an asymmetric multicomponent formulation, Contributions to Mineralogy and Petrology, 145, 492-501, 2003.

5   Holland, T. & Powell, R.: An improved and extended internally consistent thermodynamic dataset for phases of petrological interest, involving a new equation of state for solids, Journal of Metamorphic Geology, 29, 333–383, 2011.

Hollis, J. A, Harley, S. L., White, R. W., Clarke, G. L.: Preservation of evidence for prograde metamorphism in ultrahigh-temperature, high-pressure kyanite-bearing granulites, South Harris, Scotland, Journal of Metamorphic Geology, 24, 263-279, 2006.

10 Indares, A.: Eclogitized gabbros from the eastern Grenville Province: textures, metamorphic context, and implications, Canadian Journal of Earth Science, 30, 159-173, 1993.

Ings, S. J., Owen, J. V.: 'Decompressional' reaction textures formed by isobaric heating: an example from the thermal aureole of the Taylor Brook Gabbro Complex, western Newfoundland , Mineralogical Magazine, 66, 941-951, 2002.

Joesten, R.: Evolution of mineral zoning in diffusion metasomatism, Geochimica et Cosmochimica Acta, 41, 649-670, 1977.

15 Joesten, R.: The role of magmatic reaction, diffusion and annealing in the evolution of coronitic microstructure in troctolitic gabbro from Risor, Norway, Mineralogical Magazine, 50, 441-467, 1986.

Joesten, R., Fisher, G. W.: Kinetics of diffusion-controlled mineral growth in the Christmas Mountains (Texas) contact aureole, Geological Society of America Bulletin, 100, 714-732, 1988.

Johnson, C. D., Carlson, W. D.: The origin of olivine-plagioclase coronas in metagabbros from the Adirondack Mountains,
20 New York, Journal of Metamorphic Geology, 8, 697-717, 1990.

Johnson, T. E., Brown, M., Gibson, R. L., Wing, B.: Spinel-cordierite symplectites replacing andalusite: evidence for melt-assisted diapirism in the Bushveld Complex, South Africa, Journal of Metamorphic Geology, 22, 529-545, 2004.

Kelsey, D. E., White, R. W., Powell, R.: Orthopyroxene-sillimanite-quartz assemblages: distribution, petrology, quantitative P-T-X constraints and P-T paths, Journal of Metamorphic Geology, 21, 439-453, 2003a.

Kelsey, D. E., White, R. W., Powell, R., Wilson, C. J. L., Quinn, C. D.: New constraints on metamorphism in the Rauer Group, Prydz Bay, east Antarctica, Journal of Metamorphic Geology, 21, 739-759, 2003b.

Koons, P. O., Rubie, D. C., Fruch-Green, G.: The Effects of Disequilibrium and Deformation on the Mineralogical Evolution of Quartz Diorite During Metamorphism in the Eclogite Facies, Journal of Petrology, 28, 679-700, 1987.

5 Korzhinskii, D. S.: Physicochemical Basis of the Analysis of the Paragenesis of Minerals, Consultants Bureau, New York, 142, 1959.

Korzhinskii, D. S.: The theory of systems with perfectly mobile components and processes of mineral formation, American Journal of Science, 263, 193-205, 1965.

Kretz, R.: Symbols for rock-forming minerals, American Mineralogist, 68, 277-279, 1983.

10 Kriegsman, L. M., Schumacher, J. C.: Petrology of sapphirine-bearing and associated granulites from central Sri Lanka, Journal of Petrology, 40, 1211-1239, 1999.

Lal, R. K., Ackermand, D., Upadhyay, H.: P-T-X relationships deduced from corona textures in sapphirine-spinel-quartz assemblages from Paderu, southern India, Journal of Petrology, 28, 1139-1168, 1987.

Markl, G., Foster, C. T., Bucher, K.: Diffusion-controlled olivine corona textures in granitic rocks from Lofoten, Norway:
15 calculation of Onsager diffusion coefficients, thermodynamic modelling and petrological implications, Journal of Metamorphic Geology, 16, 607-623, 1998.

McFarlane, C. R. M., Carlson, W. D., Connelly, J. N.: Prograde, peak, and retrograde P-T paths from aluminium in orthopyroxene: High-temperature contact metamorphism in the aureole of the Makhavinekh Lake Pluton, Nain Plutonic Suite, Labrador, Journal of Metamorphic Geology, 21, 405-423, 2003.

20 Mongkoltip, P., Ashworth, J. R.: Quantitative estimation of an open-system symplectite-forming reaction: restricted diffusion of Al and Si in coronas around olivine, Journal of Petrology, 24, 635-661, 1983.

Mork, M. B. E.: Coronite and eclogite formation in olivine gabbro (Western Norway): reaction paths and garnet zoning, Mineralogical Magazine, 50, 417-426, 1986.

Nishiyama, T.: Steady diffusion model for olivine-plagioclase corona growth, Geochimica et Cosmochimica Acta, 41, 649-
25 670, 1983.

Norlander, B. H., Whitney, D. L., Teyssier, C., Vanderhaeghe., O.: Partial melting and decompression of the Thor-Odin dome, Shuswap metamorphic core complex, Canadian Cordillera, Lithos, 61, 103-125, 2002.

Ogilvie, P.: Metamorphic Studies in the Vredefort Dome, Unpublished Ph.D. thesis, University of Witwatersrand, Johannesburg, 772pp, 2010.

5   Osanai, Y., Nakano, N., Owada, M.: Permo-Triassic ultrahigh-temperature metamorphism in the Kontum Massif, central Vietnam, Journal of Mineralogical and Petrological Sciences, 99, 225-241, 2004.

Perchuk, L. L., Tokarev, D. A., van Reenen, D. D., Varlamov, D. A., Gerya, T. V., Sazonova, L. V., Fel'dman, V. I., Smit, C. A., Brink, M. C., Bisschoff, A. A.: Dynamic and Thermal History of the Vredefort Explosion Structure in the Kaapvaal Craton, South Africa, Petrology, 10, 395-432, 2002.

10   Powell, R., Guiraud, M., White, R. W.: Truth and beauty in metamorphic mineral equilibria: conjugate variables and phase diagrams, Canadian Mineralogist, 43, 21-33, 2005.

Powell, R., Holland, T. J. B.: An internally consistent thermodynamic dataset with uncertainties and correlations: 3: application methods, worked examples and a computer program, Journal of Metamorphic Geology, 6, 173-204, 1988.

Powell, R., Holland, T. J. B.: Calculated mineral equilibria in the pelite system KFMASH (K2O-FeO-MgO-Al2O3-SiO2-
15   H2O), American Mineralogist, 75, 367-380, 1990.

Powell, R., Holland, T. J. B., Worley, B.: Calculating phase diagrams involving solid solutions via non-linear equations, with examples using THERMOCALC, Journal of Metamorphic Geology, 16, 577-588, 1998.

Sheplev, V. S., Kolobov, V. Yu., Kuznetsova, R. P., Reverdatto, V. V.: Analysis of growth of zonated mineral segregation and characteristics of mass transfer during metamorphism. 1. Theoretical model in a quasi-stationary approximation, Soviet
20   Geol. Geophys., 32, 1-12, 1991.

Sheplev, V. S., Kuznetsova, R. P., Kolobov, V. Yu.: Analysis of growth of zonated mineral segregations and characteristics of mass transfer during metamorphism. 2. The system SiO2-Al2O3-MgO-NaCaO, Russian Geol. Geophys., 33, 73-80, 1992a.

Sheplev, V. S., Kuznetsova, R. P., Kolobov, V. Yu.: Analysis of growth of zonated mineral segregations and characteristics
25   of mass transfer during metamorphism. 3. The model of steady diffusions, Russian Geol. Geophys., 33, 46-52, 1992b.

Štípská, P., Powell, R., White, R. & Baldwin, J.: Using calculated chemical potential relationships to account for coronas around kyanite: an example from the Bohemian Massif, Journal of Metamorphic Geology, 28, 97–116, 2010.

Stüwe, K.: Effective bulk composition changes due to cooling: a model predicting complexities in retrograde reaction textures, Contributions to Mineralogy and Petrology, 129, 43-52, 1997.

5   Tajčmanová, L., Konopásek, J. & Connolly, J.A.D.: Diffusion-controlled development of silica-undersaturated domains in felsic granulites of the Bohemian Massif (Variscan belt of Central Europe). Contributions to Mineralogy and Petrology, 153, 237–250, 2007

Thompson, J. B.: Local equilibrium in metasomatic processes, in: Researches in Geochemistry, Wiley, New York, 427-457, 1959.

10   Tracy, R. J., McLellan, E. L.: A natural example of the kinetic controls of compositional and textural equilibration, in: Advances in physical geochemistry 4, Springer-Verlag, 118-137, 1985.

Tsunogae, T., Van Reenen, D. D., : Corundum + quartz and Mg-staurolite bearing granulite from the Limpopo Belt, southern Africa: Implications for a P-T path, Lithos, 92, 576-587, 2006.

Van Lamoen, H.: Coronas in olivine gabbros and iron ores from Susimäki and Riuttamaa, Finland, Contributions to 15   Mineralogy and Petrology, 68, 259-268, 1979.

Vidale, R.: Metasomatism in a chemical gradient and the formation of calc-silicate bands, American Journal of Science, 267, 857-874, 1969.

Wheeler, J., Mangan, L. S., Prior, D. J.: Disequilibrium in the Ross of Mull Contact Metamorphic Aureole, Scotland: a Consequence of Polymetamorphism, Journal of Petrology, 45, 835-853, 2004.

20   White, R. W., Powell, R.: Melt loss and the preservation of granulite facies mineral assemblages, Journal of Metamorphic Geology, 20, 621-632, 2002.

White, R. W., Powell, R.: On the interpretation of retrograde reaction textures in granulite facies rocks, Journal of Metamorphic Geology, 29, 131–149, 2011.

White, R. W., Powell, R., Baldwin, J. A.: Calculated phase equilibria involving chemical potentials to investigate the textural 25   evolution of metamorphic rocks, Journal of Metamorphic Geology, 26, 181-198, 2008.

White, R. W., Powell, R., Halpin, J. A.: Spatially-focussed melt formation in aluminous metapelites from Broken Hill, Australia, Journal of Metamorphic Geology, 22, 825-845, 2004.

Whitney, P. R., McLelland, J. M.: Origin of coronas in metagabbros of the Adirondack Mts., N.Y., Contributions to Mineralogy and Petrology, 39, 81-98, 1973.

5   Zulbati., F, Harley, S. L.: Late Archaean granulite facies metamorphism in the Vestfold Hills, East Antarctica, Lithos, 93, 39-67, 2007.
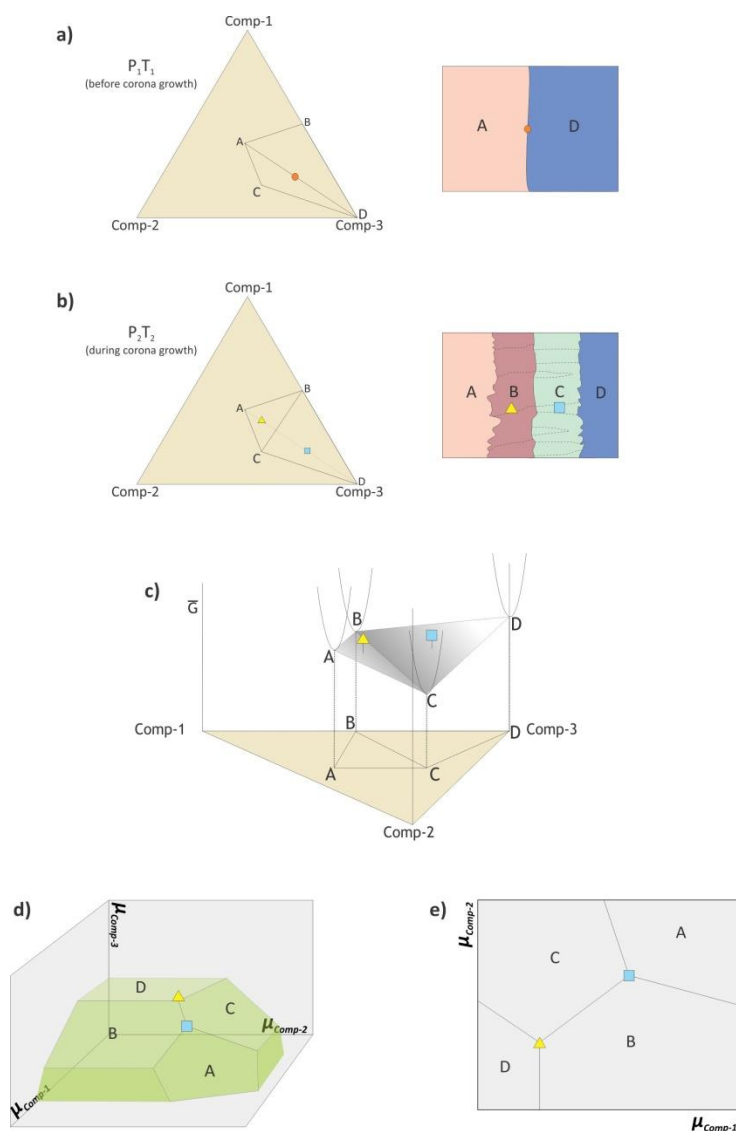
Figure 1. Chemographic relationships and chemical potential saturation surfaces for local transient equilibria at corona boundaries during incipient stages of single-stage, steady-state, diffusion-controlled corona growth (after Joesten, 1977). (a) Original phases (A and D) initially at equilibrium under P_1 and T_1 with bulk composition indicated by the circle. (b) New P and T conditions (P_2, T_2) are kinetically inhibited and reaction progress becomes diffusion-controlled. The corona domain is partitioned into a continuum of compositional subdomains, or incipient "effective bulk compositions" (triangle, square), each with unique chemical potentials, in which local equilibrium is attained. (c) Ternary G-X surface, in which local equilibria are separated by chemical potential differences. (d) The chemical potential saturation surface for each of the local phase assemblages. (e) Projection of the saturation surface on the μ_{comp1}-μ_{comp2} plane. Chemical potential gradients between local equilibria drive diffusion of components from one compositional domain to another until chemical potentials are equalised and equilibrium is attained.
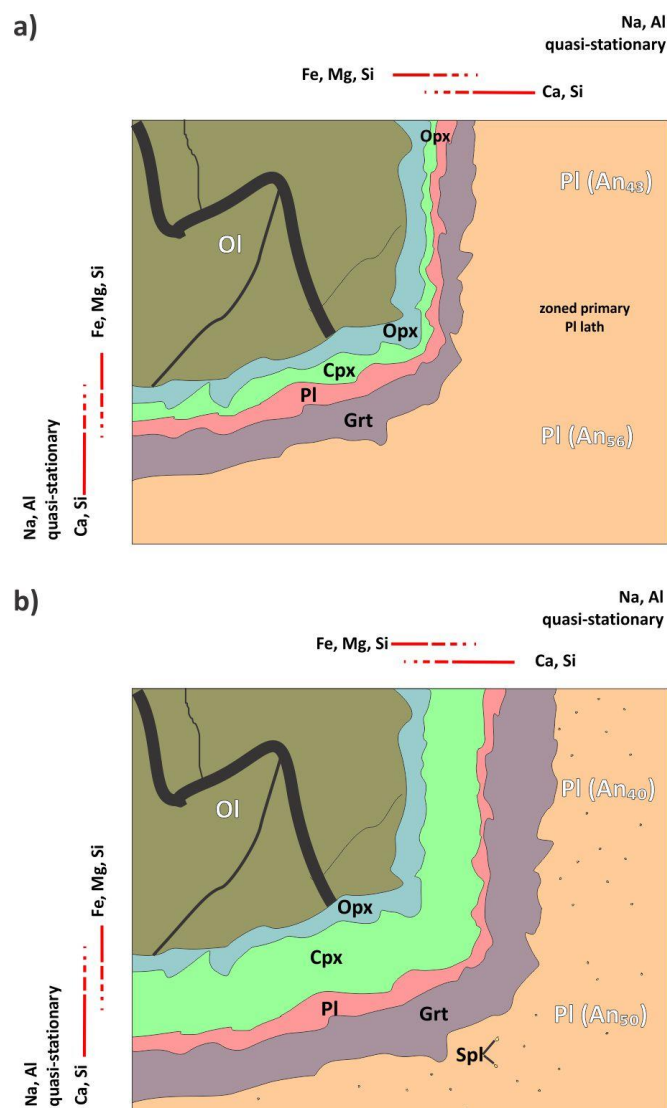
Figure 2. Open-system, continuous, single-stage, steady-state, diffusion-controlled growth of prograde corona layers between olivine and plagioclase (modified after Johnson and Carlson, 1990). (a) With incipient reaction, different rates of intergranular diffusion for major components manifest as spatially segregated layers. The corona domain is partitioned into a continuum of compositional subdomains or incipient effective bulk compositions in which local equilibrium is attained, each with unique chemical potentials. Fe, Mg and Si released from olivine diffuse down chemical potential gradients toward plagioclase, whereas Na, Ca, Al and Si released from plagioclase diffuse toward olivine. Layers comprising the slowest diffusing species (Al) adjoin the most aluminous reactant. (b) Reactions occur at layer boundaries and layers expand as diffusion progresses. The width and composition of each corona layer depend on the relative fluxes of the diffusing elements. Minor spinel clouding occurs in reactant plagioclase as Ca and Si diffuse preferentially into the reaction band, creating a Si deficiency in reactant plagioclase.
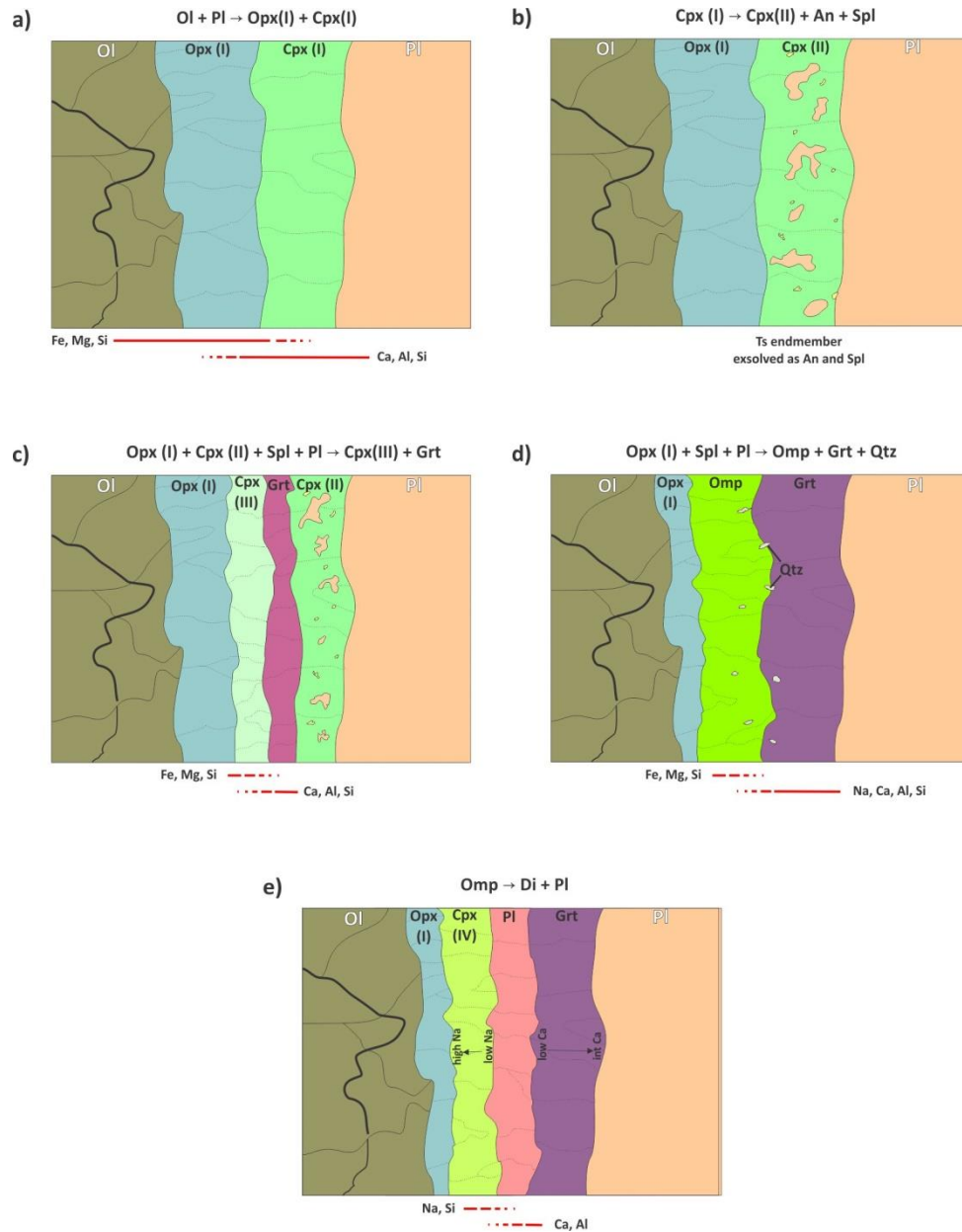
Figure 3. Non-continuous, multi-stage, sequential layer development in a corona between olivine and plagioclase formed in response to changing *P* and *T* along the *P-T* path shown in Fig. 2 (after Griffin, 1972). (a) Original olivine and plagioclase react to form orthopyroxene and clinopyroxene. (b) Clinopyroxene breaks down to form a less Tschermakitic composition with plagioclase and spinel. (c) Clinopyroxene reacts with orthopyroxene, spinel and plagioclase to produce garnet. (d) Orthopyroxene reacts with spinel and plagioclase to produce omphacite, garnet and quartz. (e) Omphacite decomposes to clinopyroxene and plagioclase.
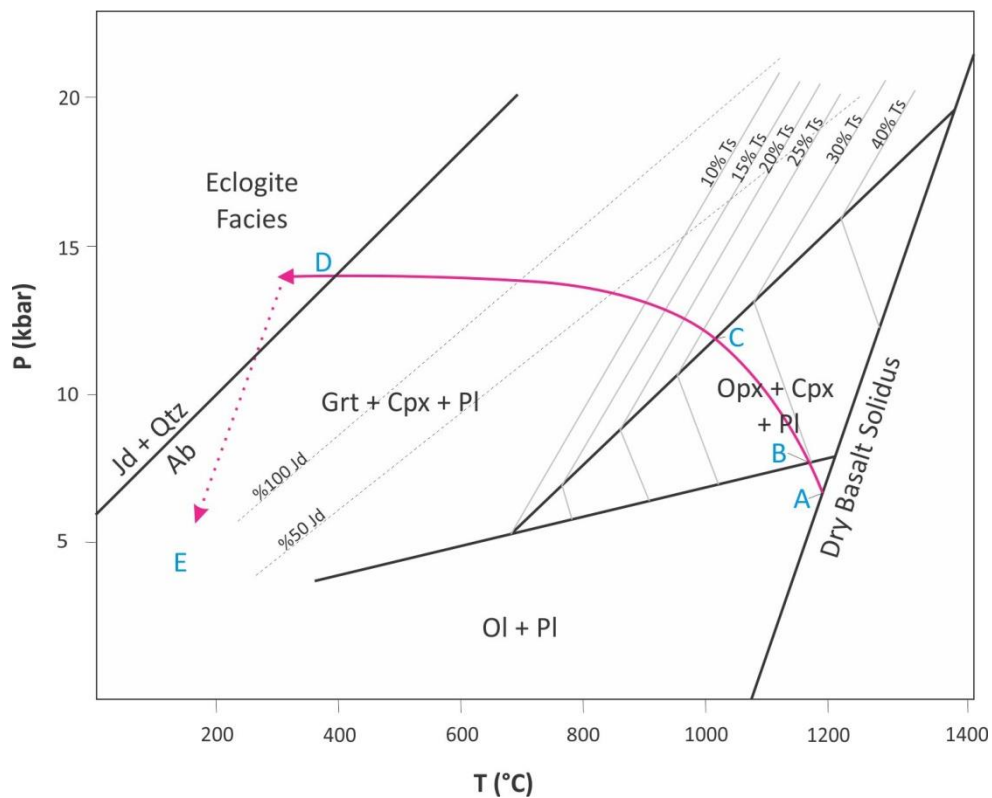
Figure 4. *P-T* grid indicating univariant equilibria crossed during cooling to produce the sequence of reactions in Fig. 1 (after Griffin, 1972).
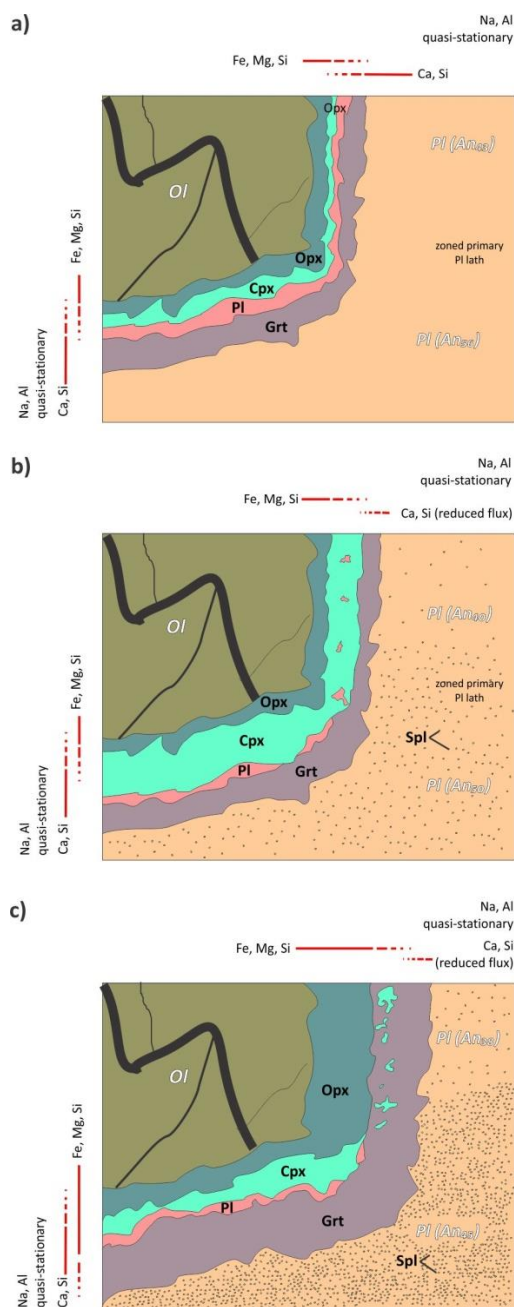
Figure 5. Non-continuous, multi-stage, sequential layer corona layer development at constant P and T in response to waning boundary fluxes of rapidly diffusing components from the reactants into the corona in an open system (after Johnson and Carlson, 1990). (a) Initial steady-state layer configuration for an olivine-plagioclase corona. (b) Depletion of Ca and Si in the reactants leads to the consumption of plagioclase, and then (c) clinopyroxene, in transient states. The system gradually evolves toward a new steady state. Cannibalisation of corona plagioclase and clinopyroxene is more enhanced where the original reactant is Ca-poor (top-right, An_{38}).
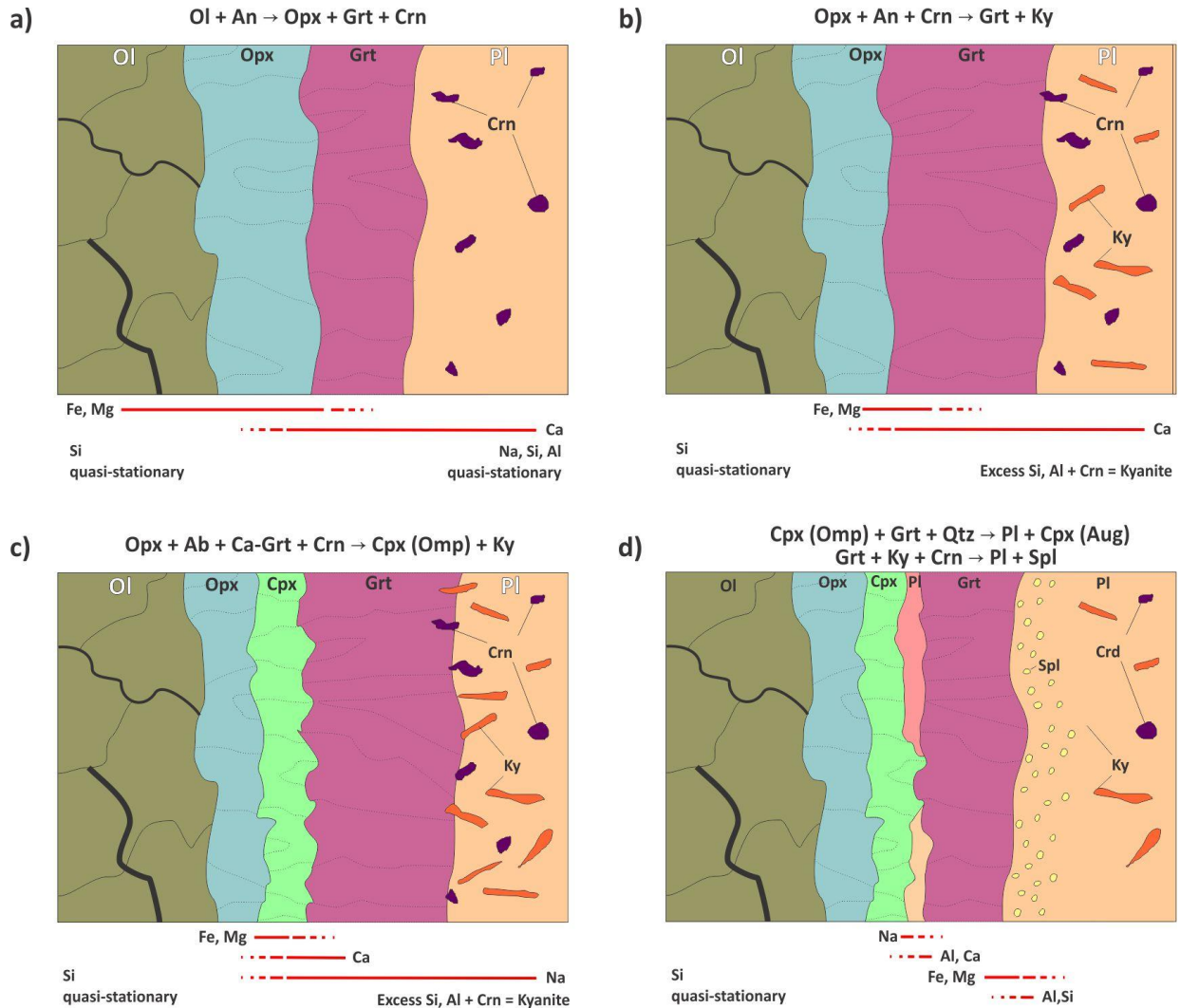
Figure 6. Non-continuous, multi-stage, sequential corona layer development between plagioclase and olivine owing to varying component fluxes across the corona bands and, later, owing to decompression (modified after Indares, 1993). Corona layer growth in (a)-(c) occurs under constant high *P* and *T*, initially from discrete reactions between reactants and then subsequently between individual corona layers as component fluxes vary across the corona. The formation of the plagioclase layer in (d) is ascribed to decompression. Detailed reaction mechanisms are discussed in the text.
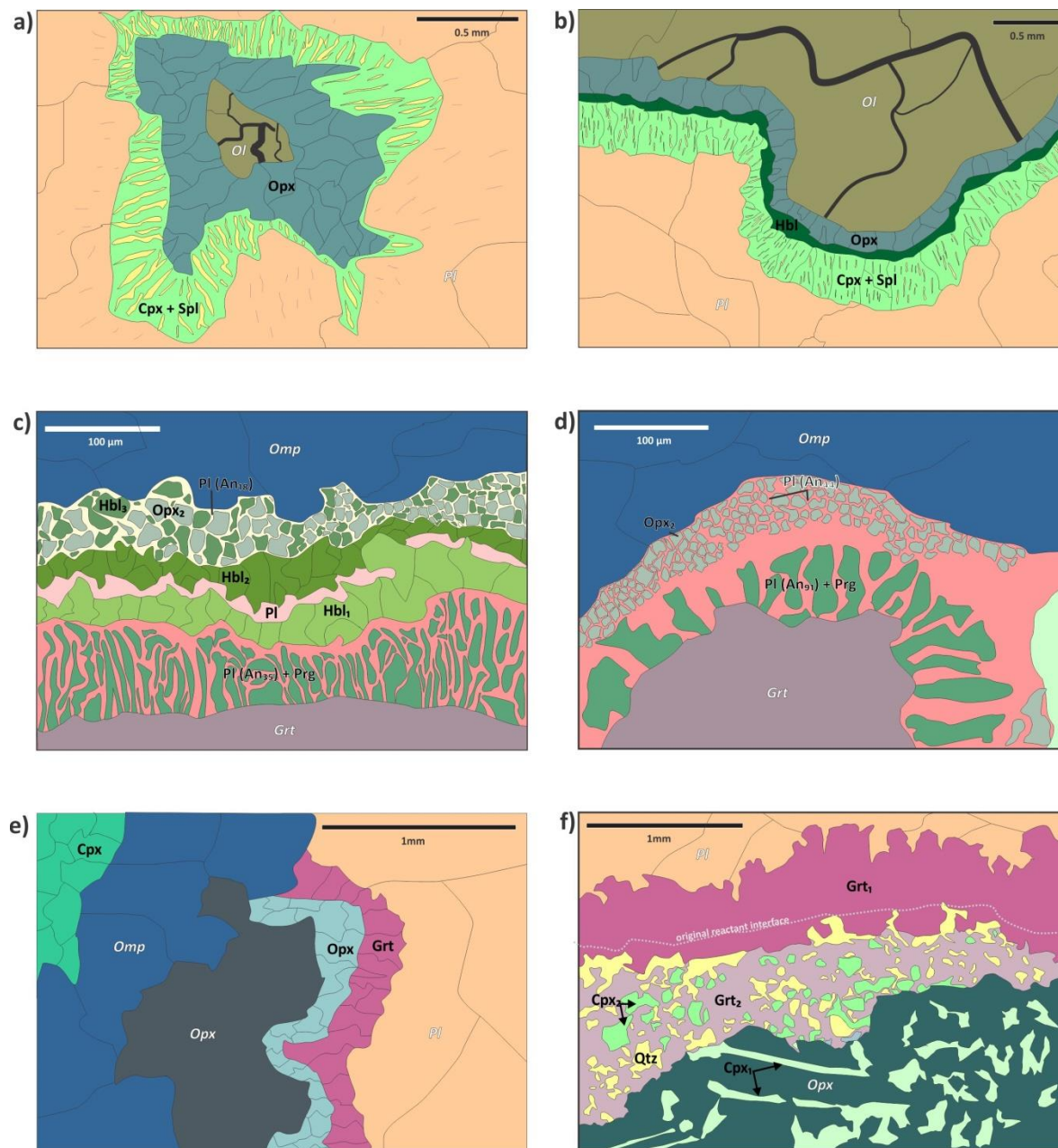
Figure 7. Common corona textures developed in mafic granulites. (a) Prograde corona developed between olivine and plagioclase during burial following shallow intrusion in the southwestern Adirondacks, New York (after Whitney and McLelland, 1973). Garnet is not present in this corona owing to low inferred pressures during corona reaction. There is no variation in X_{Mg} of pyroxenes. (b) A retrograde corona developed between olivine and plagioclase in an olivine metagabbro from northeast Scotland (after Mongkoltip and Ashworth,

1983). The presence of amphibole suggests higher $a\mathrm{H_2O}$ than in more anhydrous domainal compositions where only clinopyroxene is stable. Al content and X_{Fe} of Opx and Hbl increase toward Pl reactant. c) Retrograde corona developed between garnet and clinopyroxene during a static thermal event with the intrusion of numerous granite plutons in the Llano Uplift, Texas (after Carlson and Johnson, 1991). The presence of hornblende implies relatively high $a\mathrm{H_2O}$ during reaction. Both hornblende and plagioclase are asymmetrically zoned

5 across the corona band. Plagioclase becomes less calcic ($\mathrm{An_{35}}$ to $\mathrm{An_{18}}$) and amphibole Fe/Mg and Al/Si ratios decrease toward omphacite. (d) Retrograde corona developed between garnet and clinopyroxene from the Snowbird Tectonic Zone, Western Canadian Shield (after Baldwin et al., 2004). The restricted distribution of hornblende in this corona compared to that in (c), suggests a less hydrous bulk corona composition. Marked zonation in plagioclase occurs from $\mathrm{An_{91}}$ adjacent garnet to $\mathrm{An_{44}}$ at clinopyroxene margin. (e) Prograde corona developed between plagioclase and orthopyroxene during deformation-enhanced reaction in a dolerite towards a shear zone (after White

10 and Clarke, 1997). Garnet exhibits asymmetric zonation as X_{Alm}, X_{Prp} and X_{Grs} increase toward Pl. Garnet zoning diminishes toward shear zone. (f) Prograde corona developed between plagioclase and orthopyroxene in a mafic granulite from Yenisey Ridge, Siberia (after Ashworth et al., 1998). Layer 1 garnet ($\mathrm{Grt_1}$) is zoned: Fe increases and Ca decreases (X_{Grs}: 0.24 - 0.21; X_{Alm}: 0.54 - 0.60) toward layer 2. A slight compositional perturbation across layer 1 is thought to mark the initial Pl/Opx boundary. In layers 3 and 4, Ca in garnet is almost constant, with higher Fe and lower Mg than in layer 1. No systematic zonation is observed in pyroxene. Non-equilibrium

15 thermobarometric estimates for corona formation are 740 ± 20 °C and 9.5 ± 0.7 kbar (Ashworth et al., 2001).
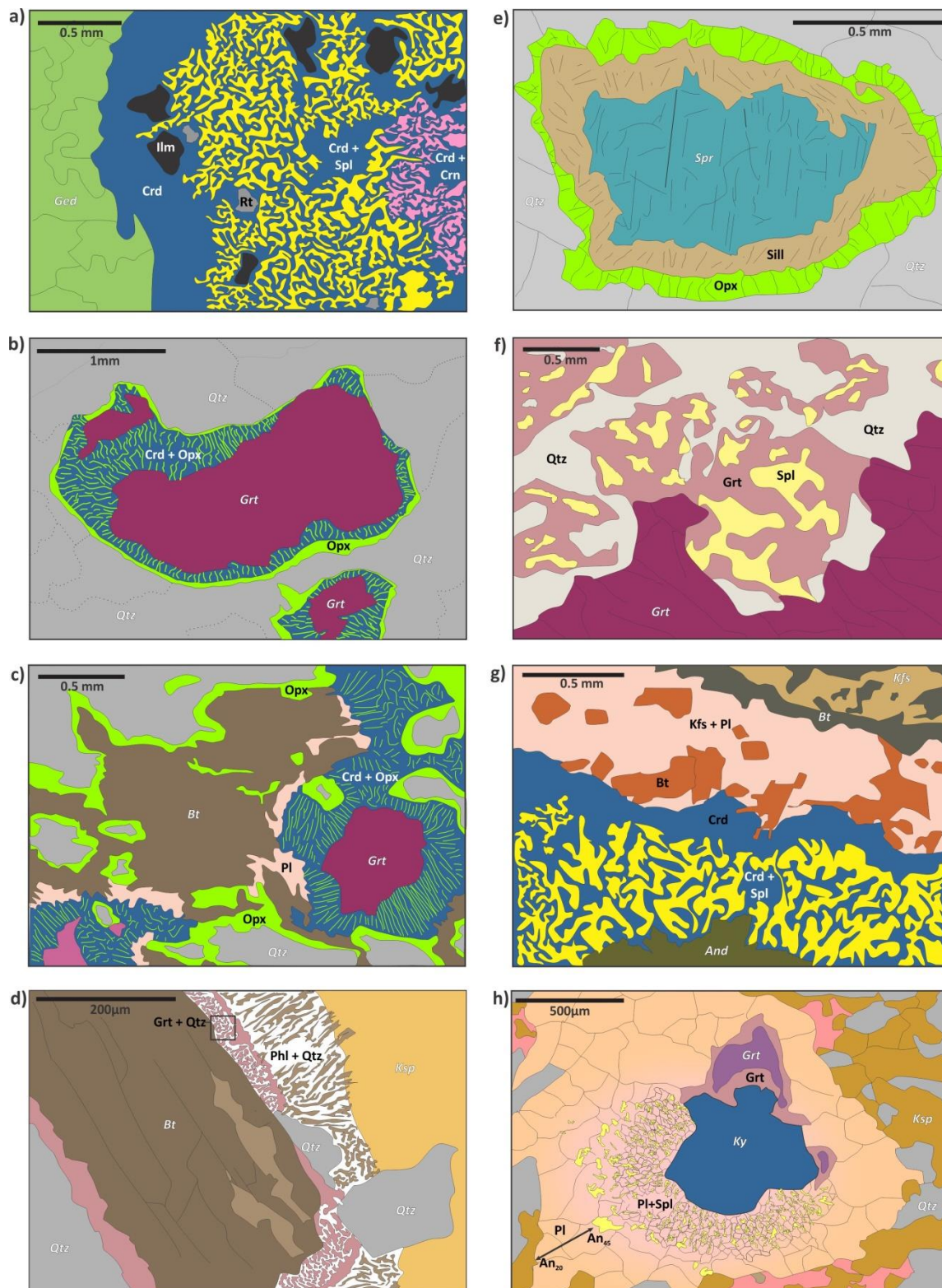
Figure 8: Sectoral complexity in corona textures developed in pelitic granulites. (a) Complex corona between kyanite and gedrite (after Norlander et al., 1996). No compositional variation in any corona phases was observed. Conditions of formation constrained at < 5 kbar and ~ 750 °C with TWQ and conventional thermobarometers. (b) Common complex corona developed after garnet and quartz (after Hollis et al., 2006). No systematic variation is described in corona products. (c) Complex sectoral corona between garnet, biotite and quartz. Monomineralic plagioclase is constrained to the corona immediately adjacent to biotite. Similarly, blocky orthopyroxene occurs only in the corona sectors where garnet reacts with quartz (after Kelsey et al., 2003b). Cordierite X_{Mg} varies across symplectite increasing toward orthopyroxene in general. No variation in orthopyroxene composition is observed. (d) Symplectite-dominated corona developed between biotite and K-feldspar (after Bruno et al., 2001). Where biotite reacts with quartz, monomineralic garnet comprises the corona. Elsewhere, a complex, symplectite-dominated corona comprising garnet, quartz and phlogopite occurs where biotite and feldspar react. Corona garnet is weakly zoned. (e) Monomineralic sillimanite and orthopyroxene developed after sapphirine and quartz (after Ellis et al., 1980 and Grew, 1980). (f) Retrograde spinel-garnet symplectite replacing peak garnet during post-peak decompression (after White et al., 2002). This corona develops in response to changing modes in a high variance equilibrium assemblage. No univariant reaction is crossed. (g) Prograde complex corona comprising spinel-cordierite symplectite and leucocratic biotite, K-feldspar and plagioclase after andalusite (after Johnson et al., 2004). X_{Mg} of cordierite decreases toward biotite (0.55 - 0.51) with no variation in spinel composition. Cordierite moat formation occurs during an andalusite melting reaction consuming quartz and biotite, followed by continued breakdown of andalusite to cordierite-spinel symplectite in SiO_2 deficient domains. (h) Sectoral replacement of kyanite by plagioclase+spinel symplectite and zoned monomineralic plagioclase. Where primary garnet abuts kyanite, the symplecittie is not developed, and kyanite is replaced by low-Ca garnet enclosed by unzoned plagioclase (After Štípská et al., 2009).
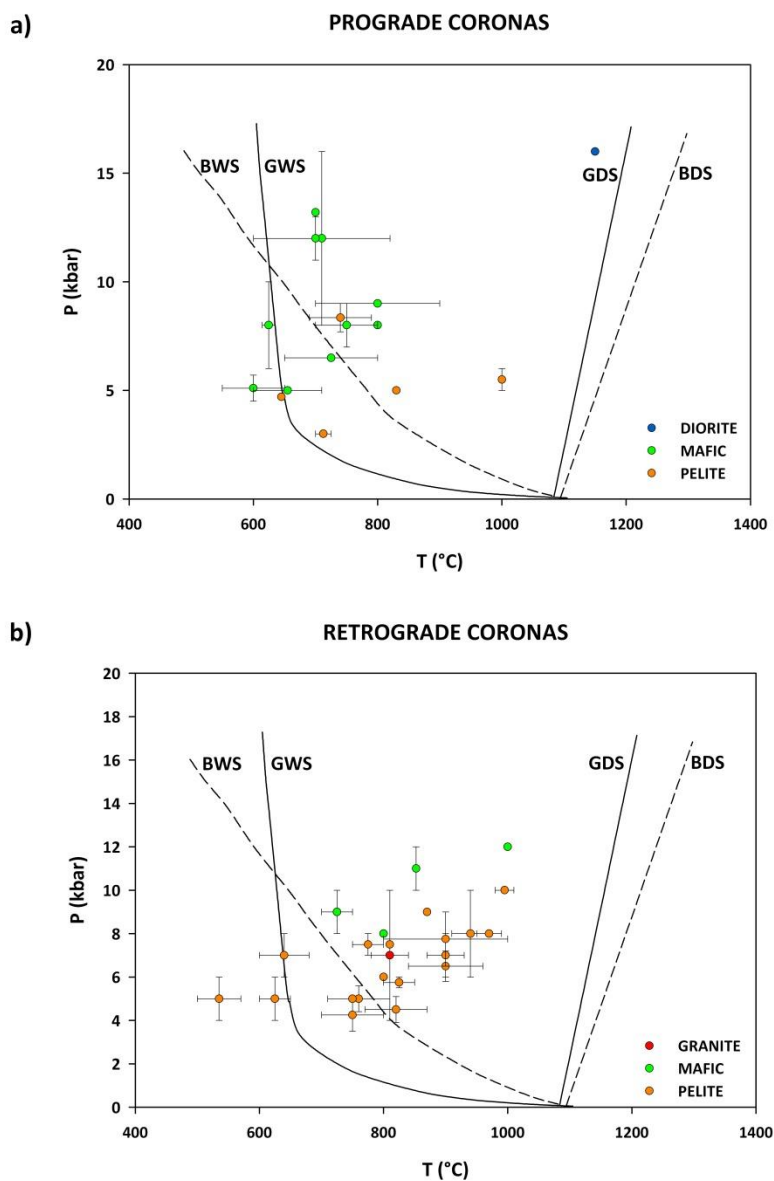
Figure 9: Summary of *P-T* conditions of formation for coronas reviewed in this study. (a) *P-T* conditions for prograde coronas. (b) *P-T* conditions for retrograde coronas. In general, conditions of corona formation occur above the wet solidus for each respective bulk composition. The few coronas that plot at lower temperatures than the wet solidi may be subject to retrograde diffusional resetting of the thermometers and, in reality, may have formed at higher suprasolidus temperatures. Error bars are for the range of each estimate. BWS = wet basalt solidus; GWS = wet granite solidus; GDS = dry granite solidus and BDS = dry basalt solidus. Solidi were digitised in *P-T* space from geosciences resource database available at **http://www.geosci.usyd.edu.au/users/prey/Granite/Granite.html**
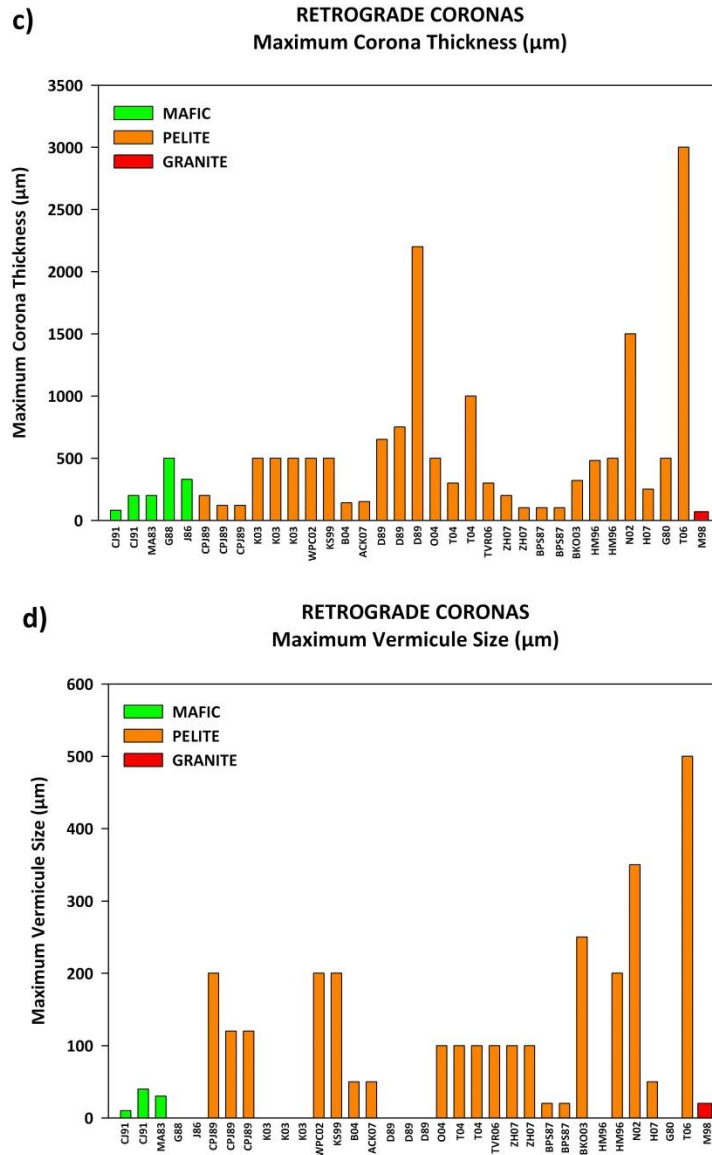
Figure 10: Variation in corona microstructure in mafic and pelitic bulk rock compositions. (a) Variation in maximum corona thickness in prograde coronas. (b) Variation in maximum vermicule size in prograde coronas. Hatched bars are prograde coronas from contact aureoles. Each corona reference is tagged by a code (e.g., WM73) which correlated with the detailed charactersitics of each corona in the Tables included in Appendix1.
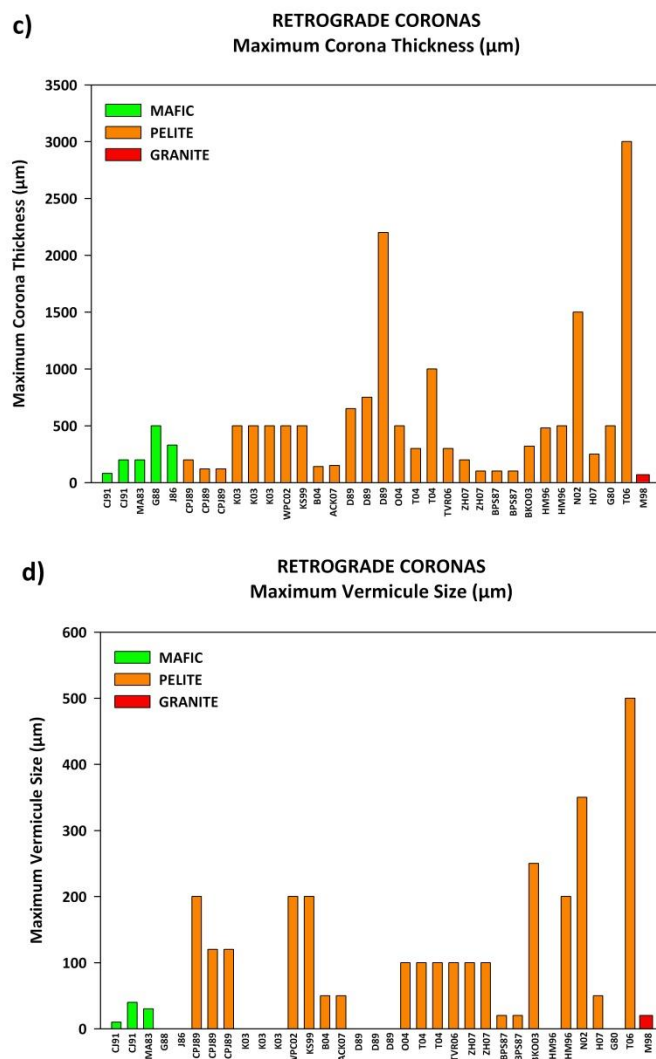
Figure 11: Variation in corona microstructure in mafic and pelitic bulk rock compositions. (c) Variation in maximum corona thickness in retrograde coronas. (d) Variation in maximum vermicule size in retrograde coronas.
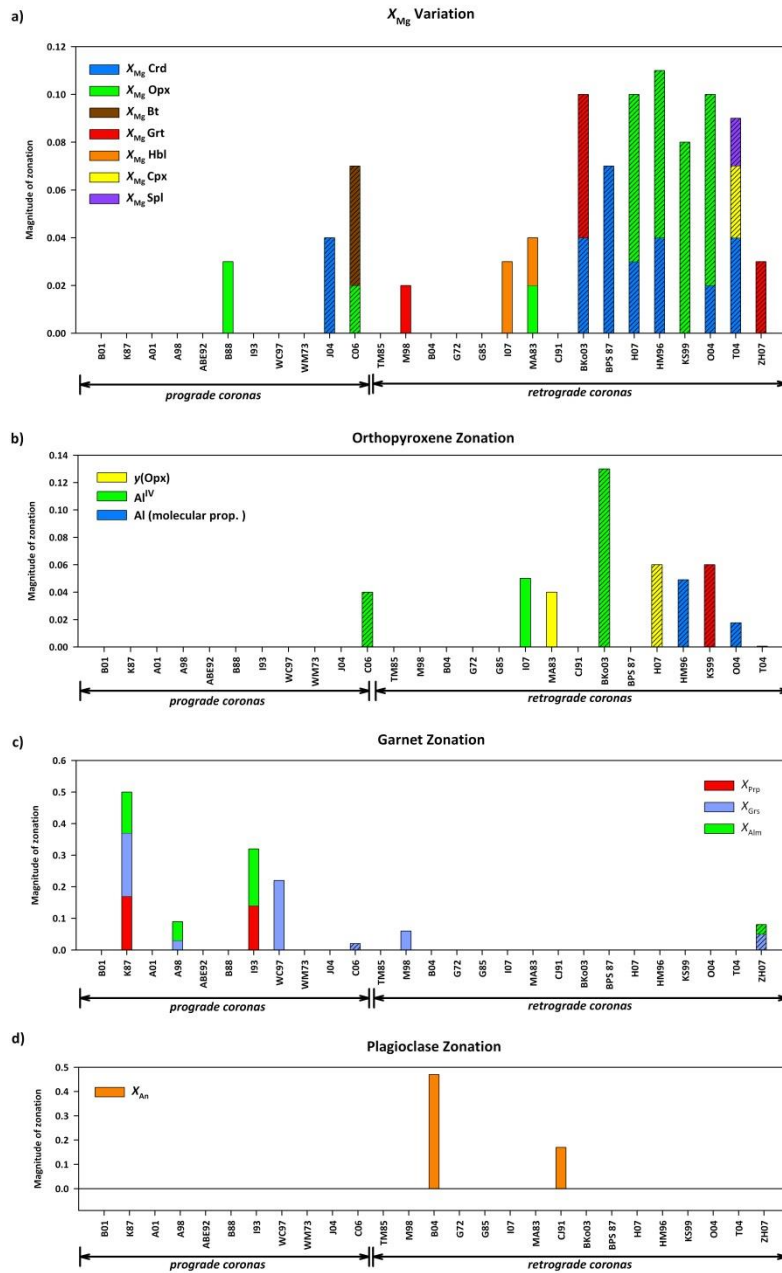
Figure 12: Magnitude of compositional zonation in product corona bands. Hatched fields indicate pelitic bulk rock compositions; unhatched are mafic. (a) X_{Mg} variation in product phases. (b) Variation in Al content in orthopyroxene across each corona (c) Garnet zonation across each corona. (d) Plagioclase zonation across coronas where it is documented.

Figure 13: Sketch of a typical corona developed between plagioclase and olivine in metagabbros (after Ashworth, 1993). As reaction proceeds, layers grow by diffusion along grain boundaries of requisite components down concentration gradients to layer boundaries where they are consumed in the production of product phases. Al is considered to be the most immobile diffusing species, since Al concentration gradients are most marked. Al exerts the greatest control on segregation of corona products in bands, from the most Al-rich symplectite adjacent to plagioclase to Al-poor orthopyroxene adjacent to olivine.
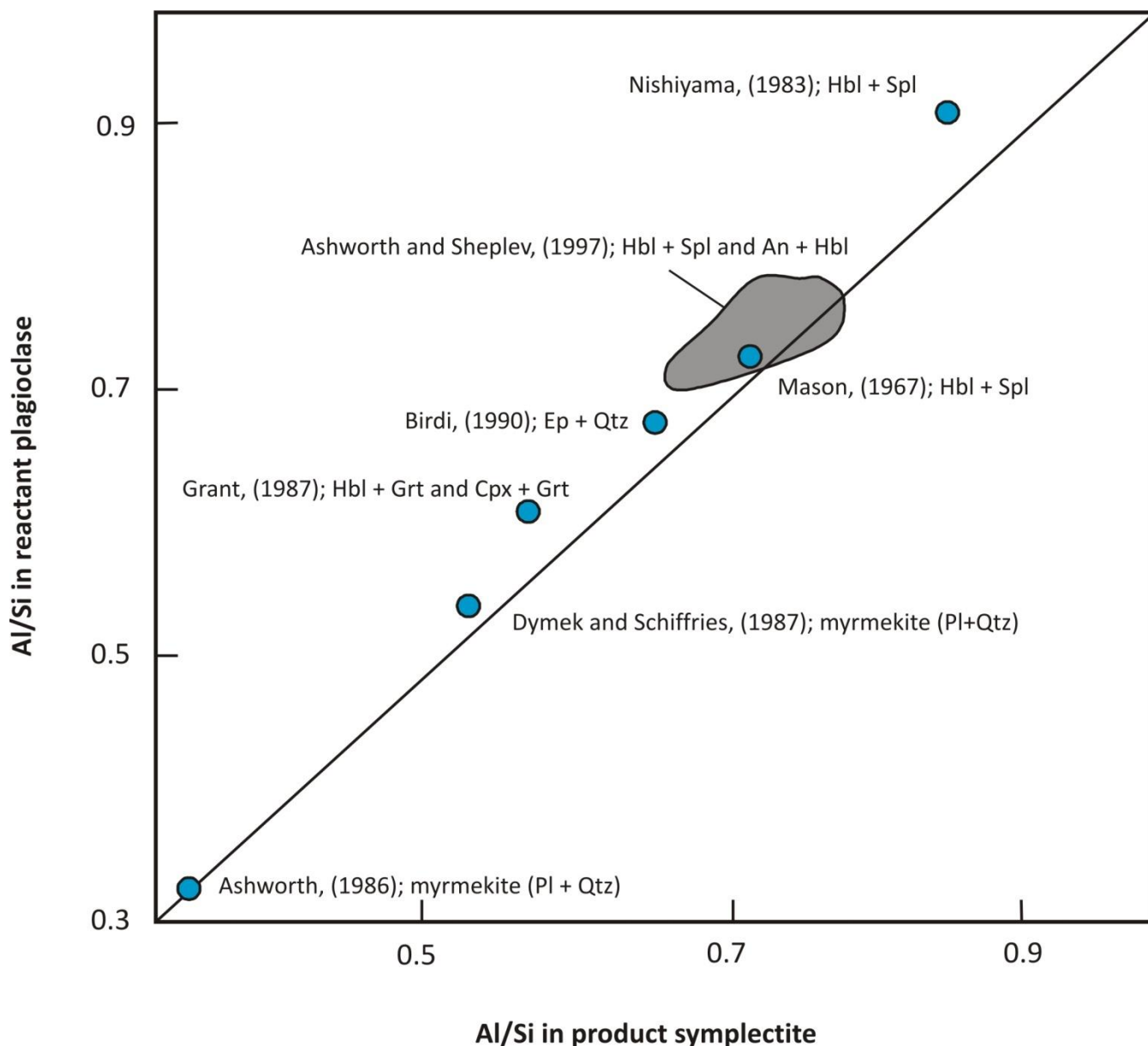
Figure 14: Isocon plot of Al/Si ratios in symplectites and the adjacent reactant plagioclase. The isocon line represents Al/Si ratios that are preserved exactly between reactant and products. Any deviation from this line indicates a degree of open-system behaviour. In general, analysed symplectites from the literature plot above the isocon line, suggesting that the Al/Si ratio is lower in the product symplectite than it is in the reactant plagioclase, i.e., the corona system is losing Al to the external system relative to Si with prolonged reaction.
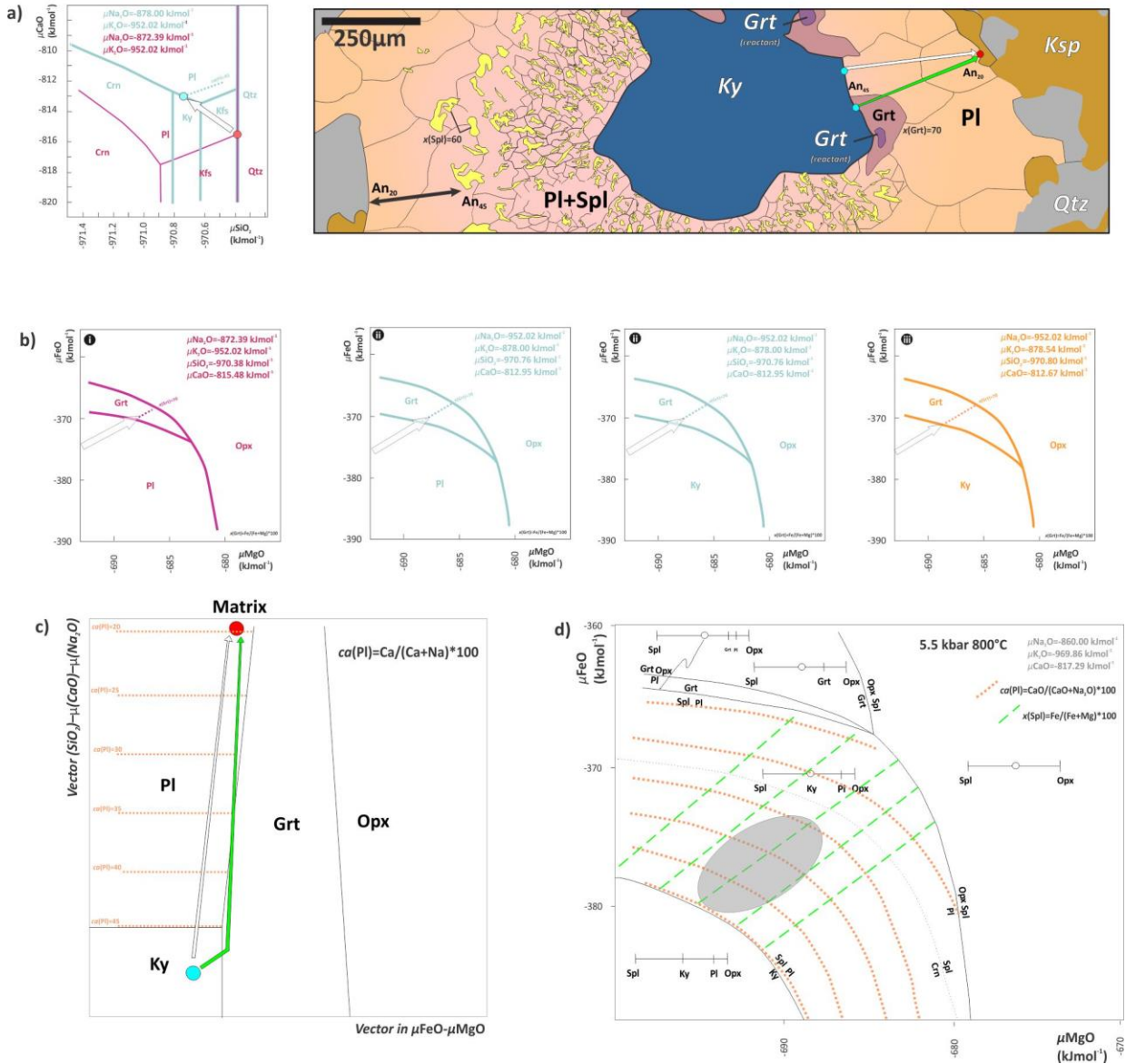
Figure 15: Chemical potential relationships governing the development of a corona after kyanite (after Štípská et al., 2009). (a) Calculated $\mu(SiO_2)$– $\mu(CaO)$ diagrams in the NCKAS system for the matrix (red lines) and the kyanite boundary (light blue lines). Gradients in the chemical potentials from the matrix to the kyanite–plagioclase boundary are represented by a vector in $\mu(SiO_2)$–$\mu(CaO)$–$\mu(Na_2O)$ space.

5   (b) Superimposed $\mu(MgO)$ and $\mu(FeO)$ variations on the $\mu(SiO_2)$–$\mu(CaO)$–$\mu(Na_2O)$ vector from (a): (i) for the matrix, (ii) for the plagioclase–kyanite boundary and (ii) inside kyanite. The topology shows garnet and orthopyroxene fields while spinel is metastable. Garnet compositional isopleths $x(Grt)$ are plotted within the garnet stability field. The arrow is a vector coincident with the $x(Grt) = 70$ isopleth, where $x(Grt) = Fe \, / \, (Fe + Mg) * 100$. (c) Phase topology obtained by manual combination of the calculated phase relations along

a slice at approximately fixed μ(MgO) ⁄ μ(FeO) (along x(g) = 70) from (b) with the calculated phase relations along the vector μ(SiO2)–μ(CaO)– μ(Na2O) from (a), contoured with compositional isopleths ca(pl). The dashed arrow shows a path from kyanite across garnet and plagioclase towards the matrix. (d) μ(FeO)–μ(MgO) diagrams along the ca(Pl)=45 line calculated at 800°C and 5.5 kbar. SiO_2 and Al_2O_3 are immobile. Fields are labelled with Al_2O_3–SiO_2 bar diagrams and contoured for x(Grt), x(Spl) and ca(Pl). Grey ellipses show regions of

5   plagioclase–spinel symplectite where mineral compositions correspond to observed values (ca(Pl) = 35–45 mol.% and x(Spl) = 60–63).

Appendix 1

Table 1: Summary of prograde corona occurrences in the literature

Tag	Bulk comp	Location	Reactants	Corona product assemblage	Corona Thickness, Vermicule size, Vermicule spacing	Equilibration	P, T of corona formation	Inferred P-T path	Layer growth model	Diffusion model	Comments
JC90	Olivine metagabbro	Adirondack Mountains, New York	Ol - Pl	Ol | Opx| Cpx| Grt | Pl Ol | Opx+Cpx | Pl | Grt | Pl	Corona thickness: 250 μm Vermicule size: 4 - 50 μm Vermicule spacing: 8 μm (measured from BSE images) Vermicule Shape: Columnar Opx and Grt (cannibalised Pl and Cpx - vermicular) Orientation: Columnar grains oriented perpendicular to grain boundaries	Complete - no variation in composition of corona product phases.	Assuming pressure of 8 kbar. Grt-Cpx (Ellis and Green, 1979) thermometer: Northern Adirondacks: 881 °C Southern Adirondacks: 708 °C	IBC, anti-clockwise	SSDC - gradual exhaustion of Pl as a reactant	Open: L ratios not constrained tightly	Formation at high pressure and low dH₂O. As Cu is depleted in reactant plagioclase, product plagioclase and clinopyroxene are 'cannibalised'. Geochronological evidence negates a magmatic origin and cooling from igneous temperatures at high pressures as a cause of reaction and, instead, invokes a much younger superimposed metamorphic event (cf. Whitney and McLelland, 1973).
N83	Olivine metagabbro	Mt Ikoma, Osaka, Japan	Ol - Pl	Ol | Opx | Hbl+Spl symp | Pl	Corona thickness: 50 - 300 μm Opx: < 30 μm Hbl+Spl: < 60 μm Vermicule size: -- Vermicule spacing: -- Vermicule Shape: Hbl - fibrous rods and needles, Spl - vermicular Orientation: Vermicules and rods perpendicular to layer boundaries	Disequilibrium - no systematic variation is observed.	Amphibolite facies - no quantitative thermometry.	Not specified	SSDC	Closed: L₀/L₀₃₃ >1 and L₀/L₀₃₃ > L₀₀₀/L₀₃₃	
J04	Metapelite	Phepane Dome, Bushveld Complex Aureole	And - Bt+matrix	And | Crd+Spl symp | Crd | Kfs+Pl+Bt leucosome | 35mol% fringe Bt +15mol% matrix Crd, Kfs, Qtz, Bt	Corona thickness: Crd+Spl symp < 1 mm; Crd: < 0.5 mm Vermicule size: 0.01 - 0.25 mm Vermicule spacing: -- Vermicule Shape: Crd - granoblastic-polygonal, Spl - vermicular; vermicules perpendicular to layer boundaries	Disequilibrium. X₍ₘ₎ of Crd decreases toward Bt (0.55 - 0.51); no variation in spinel composition.	700 - 725 °C, 3 kbar (P-T-X relationships from pseudosection)	Clockwise	SEQ	None	Crd moat formation during And + Bt melting reaction consuming quartz, followed by continued breakdown of And to Crd-Spl symplectite in SiO₂-deficient domains.
WC97	Dolerite	Western Musgrave Block, Australia	Corona 1: Opx - Pl Corona 2: Cpx - Pl Corona 3: Cpx - Pl Corona 4: Ilm - Pl	Corona 1: Opx | ±Pl₂ | Grt | Pl Corona 2: Cpx | Cpx₂ | Grt | Pl Corona 3: Cpx | Cpx₂ | Hbl | Pl Corona 4: Ilm | Bt | Grt+Bt symp | Grt | Pl	Corona thickness: Corona 1: 0.25 mm Corona 2: < 0.5 mm Corona 3: < 0.2 mm Vermicule size: < 10 - 125 μm Vermicule spacing:-- Vermicule Shape: Columnar Opx and subhedral, elongate Grt and Hbl oriented perpendicular to layer boundaries	No systematic variation in composition of Hbl, Pl and Cpx. Garnet asymmetric zoning: X₍ₐₗₘ₎, X₍ₚᵧ₎ and X₍ₛₚₛ₎ increase toward Pl (X₍ᵧᵣₒ₎ = 0.18 - 0.24 to grossular peaks of up to X₍ᵧᵣₒ₎ = 0.4). Grt zoning diminishes toward shear zone.	T ~ 750 °C and 12 - 14 kbar (core and rim compositions used in average P-T mode in THERMOCALC based on two assemblages: Grt, Pl, Cpx, Qtz and Grt, Pl Hbl, Qtz.	-	Hybrid SSDC	None	Equilibration is enhanced in high strain domains via a reduction in grain size leading to an increase in intergranular area, enhanced intracrystalline diffusion and nucleation, increased permeability and fluid access (White and Clarke, 1997).
J93	Olivine gabbro	Shabogamo Intrusive Suite, Eastern Grenville Province	Corona 1: Ol - Pl Corona 2: Opx - Pl	Corona 1: Ol | Opx+Cpx | Pl | Grt | Pl Corona 2: Opx | Cpx | Grt | Pl	Corona thickness: Corona 1: < 1 mm Corona 2: < 4 mm Vermicule size: -- Vermicule Shape: Granoblastic-polygonal with no preferred orientation	Asymmetrical zonation in Grt (X₍ₐₗₘ₎ 0.4 - 0.58 and X₍ₚᵧ₎ 0.17- 0.24) from Pl toward Opx. Layers more calcic in cores. No systematic zoning in Cpx. Opx homogeneous.	T ~ 700 - 800 °C and 16 kbar (core and rim compositions used) by Grt-Cpx-Pl-Qtz thermobarometry	Clockwise with steep ITD	SEQ	-	-
JF88	Chert-calc-silicate nodules in marble	Christmas Mountains, Texas (aureole enclosing alkali gabbro)	Cal - Qtz	Cal | Wo | Qtz (102 - 125m from gabbro) Cal | Tilleyite | Wo | Qtz (23 - 15m from gabbro) Cal | Spurrite | Wo | Qtz (13 - 0m from gabbro)		No compositional variation in corona products possible.	No pressure estimate. Thermal gradient (from numerical models of cooling pluton) ranges from 600 °C (15m from contact) to 1030 °C (at contact)	-	SSDC	Closed: L₍Cal₎/L₍Wo₎= 42 and L₍Cal₎/L₍CO2₎ > 1	Numerical modelling of diffusion controlled mineral growth in the aureole, yielded kinetic coefficients for non-isothermal processes.

Table 1 continued: Summary of prograde corona occurrences in the literature

Tag	Bulk comp	Location	Reactants	Corona product assemblage	Corona Thickness, Vermicule size, Vermicule spacing	Equilibration	P, T of corona formation	Inferred P-T path	Layer growth model	Diffusion model	Comments
ABE92	Basic orthogneiss	Jotun Nappe Complex, Norway	Ol - Pl	Ol | Opx/Tlc | Hbl | Hbl+Spl symp | Ep+ Hbl+Spl symp | Ep+Ts+Spl symp | Ep+Ts+Ky symp | Pl	Corona thickness: < 160 μm; Vermicule size: Not resolvable; Vermicule spacing: --; Vermicule Shape: Granoblastic-polygonal/interlobate epidote, spinel + hornblende needles/rods; Orientation: Needles weakly oriented perpendicular layer boundaries	Disequilibrium. Hbl Al/Si ratios decrease toward olivine. No systematic variation in Fe/Mg ratio of Spl and Hbl (ΔAl = 3.13 - 3.74 a.p.f.u; ΔMg = 2.17 - 2.97 a.p.f.u).	Epidote-amphibolite facies. No quantitative thermobarometry	ITD	SSDC	Open: $L_{FeO} > L_{Mg} > L_{SiO_2} \geq L_{CaO} > L_{Al} \geq L_{Ks}$	Srt+Ky and Ky+Hbl stable in H_2O-undersaturated conditions
K87	Quartz Diorite	Sesia Zone, Western Alps	Bt - Matrix	Bt | Ms | Grt | Matrix (Jd+Qz+Zo)	Corona thickness: 100 μm; Vermicule size: < 50 μm; Vermicule spacing: --; Vermicule Shape: Granoblastic-polygonal	Disequilibrium. X_{Ms} and X_{Prp} increase and X_{Grs} decreases in garnet toward biotite (X_{Alm}: 0.6 - 0.73; X_{Prp}: 0.10 - 0.17; X_{Grs}: 0.30 - 0.10).	Eclogite facies	Clockwise	SSDC	-	Domanial equilibration (extent of which is determined by the amount of deformation) and wide variation in composition of peak phases precludes application of thermobarometry
WM83	Metagabbro, metatroctolite	Adirondack Mountains, New York.	Um - Pl	Hbl | ±Bt | ±Hbl | ±Grt | Pl	Corona thickness: < 100 μm; Garnet vermicule size: < 50 μm; Vermicule spacing: --; Vermicule Shape: Columnar Opx and Bt oriented perpendicular layer boundaries	No systematic zoning observed.	700 - 800°C and 8 ± 1 kbar from equilibrium assemblages in host rocks	No P-T path suggested	SEQ	-	Open system invoked for mass balance. Polymetamorphic history, with a high pressure event following low pressure metamorphism.
B01	Granodiorite	Dora-Maira Massif, Western Alps	Corona 1: Bt - Qz; Corona 2: Bt - Kfs; Corona 3: Bt - Pl	Corona 1: Bt | Grt | Qz; Corona 2: Bt | Grt | Grt+Qz | Phg+Qz | Kfs; Corona 3: Bt | Grt | Grt+Jd | Pl	Corona thickness: Corona 1: 5 - 40 μm; Corona 2: Layer 1: 10 - 120 μm; Layer 2: 60 μm; Layer 3: 100 μm; Corona 3: Layer 1: -; Layer 2: < 50 μm; Garnet vermicule size: 2 - 50 μm; Vermicule spacing: --; Vermicule Shape: Vermicular garnet to rod-like Plg; Orientation: Perpendicular layer boundaries	Disequilibrium. Corona 1: Garnet weakly zoned (no more detail provided). Corona 2: Garnet weakly zoned (no more detail provided). Corona 3: Garnet asymmetrically zoned with Ca increasing and Fe+Mg decreasing toward Pl.	Eclogite facies. Minimum conditions of: 650 °C and 24 kbar, based on comparison between measured and modelled equilibrium compositions of garnet	Clockwise	SSDC	-	Sectoral corona development around biotite depending on immediately adjacent phase. Each corona type represents different P-T conditions at which that corona-forming reaction is overstepped.
A98	Metabasic granite	Yenisey Ridge, Siberia	Pl - Pgt (now Opx+Cpx)	Pl | Grt | Grt+Qz | Cpx+Qz+Grt | Pgt (Opx+Cpx exsolution)	Corona thickness: Layer 1: 440 μm; Layer 2: 150 μm; Layer 3: 300 μm; Vermicule size: 10 - 300 μm; Vermicule Shape: Granoblastic-polygonal/interlobate and locally needle/rod-like pyroxenes. Orientation: None.	Disequilibrium. Layer 1 Grt is zoned: Fe increases and Ca decreases (X_{Grs}: 0.24 - 0.21; X_{Alm}: 0.54 - 0.60). In layers 3 and 4, Grt X_{Grs} is constant, while X_{Py} is higher than in layer 1. No systematic zonation in pyroxene observed.	Layer 4 Grt-Opx and Grt-Opx pairs yield 614 - 635 °C (at 6 - 10 kbar (retrograde diffusional resetting). Al content in Opx, yields poorly constrained, slightly higher temperatures. Layer 4 Grt, Opx and Pl reactant yields a pressure estimate of 5.8 - 7.5 kbar (Grt-Opx-Pl-Qz; Bhattacharya et al., 1991).	Clockwise	SSDC	Open: $L_{Fe} \approx L_{Mg} \approx L_{Ca} > L_{Al} \approx L_{Si}$	The geobarometry is compromised by chemical potential gradients between phases in layer 4 and Pl reactant.
WM73	Metagabbro	Adirondacks, New York	Ol - Pl	Southwestern Adirondacks: Ol | Opx | Cpx+Spl symp | Pl	Corona thickness: < 0.25 mm; Vermicule size: 0.01 - 0.25 mm; Vermicule spacing: --; Vermicule Shape: Vermicular symplectite and columnar Opx laths; Orientation: Strongly oriented perpendicular to layer boundaries	No variation in X_{Mg} of pyroxenes.	Southwestern Adirondacks: marginally > 8 kbar and 800°C	Clockwise	SSDC?	-	-

Table 1 continued: Summary of prograde corona occurrences in the literature

Tag	Bulk comp	Location	Reactants	Corona product assemblage	Corona Thickness, Vermicule size, Vermicule spacing	Equilibration	P, T of corona formation	Inferred P-T path	Layer growth model	Diffusion model	Comments
A01	Hornblendite xenoliths in marble	Ivrea zone, Northern Italy	Hornblende - Marble	Hbl+Grt+Cpx | Cpx | Grt+Cpx | Sqr+Cpx | Cal	Corona thickness: Layer 1: 1 - 4 cm; Layer 2: 3 - 12 cm; Layer 3: < 2 cm; Vermicule size ~ 1 mm; Vermicule Shape: Granoblastic-interlobate except at layer boundaries where vermicular symplectite occurs; Preferred Orientation: Vermicular symplectite strongly oriented perpendicular to layer boundaries, otherwise none	Disequilibrium. X_{Mg} (0.8 - 0.55) and Tschermak's content in Cpx decreases toward Cal. No variation in Grt composition.	700 - 900 °C and 7 - 10 kbar (independent estimates of peak conditions from pelites)	-	SSDC	Open. A number of mass balance scenarios proposed based on qualitative evidence to constrain boundary fluxes. $L_{SiO}/L_{CaO} > 2.5$ and $L_{FeO}/L_{CaO} < 10$ and $L_{MgO}/L_{CaO} > 1$	Abart et al. (2001) relaxed the constant volume or closure to certain components assumptions to evaluate the overall reaction. Rather, they constrained a range of mass balance scenarios for which major element fluxes across mass boundaries were solved.
BB88	Metapelite and Norite	Hoggar-Iforas granulite unit, Mali	Corona 1: Grt - Sil; Corona 2: Grt - Qtz	Corona 1: Grt | Crd | Crd+Spl | Sil; Corona 2: Grt | Opx+Pl symp | Grt:+Qtz | Qtz	Corona thicknesses: Corona 1: < 80µm; Corona 2: < 700 µm; Vermicule size: 5 - 50 µm; Vermicule spacing: –; Vermicule Shape: Vermicular symplectite and granoblastic-polygonal/interlobate monomineralic layers; Preferred Orientation: Vermicular symplectite weakly oriented perpendicular to layer boundaries, otherwise none	Corona 1: No zoning in Crd or Spl. Garnet X_{Fe} decreases rimward. Corona 2: No systematic zonation. Opx: X_{Mg} = 0.65 - 0.70. X_{Al} = 0.29 - 0.32 and X_{Cr} = 0.01 - 0.02.	550 - 650 °C and 4.5 - 5.7 kbar (thermobarometry using the assemblage Grt-Spl-Crd-Bt-Pl)	Clockwise isothermal	SEQ	-	The first stage of corona growth involves breakdown of Grt to form Crd + Spl symplectites in the metapelites and Opx + Pl symplectites in the norites. Replacement of Crd + Spl by younger Grt and Sil, as well as the replacement of Opx and Pl symplectite by Grt + Qtz suggests renewed burial. Thermobarometry yields P-T conditions of the latter event. P-T path reflects Eburnean decompression, followed by Pan African burial.
C06	Metapelite	Huangtuling granulite, Northern Dabie Orogen, Eastern China	Corona 1: Bt - Pl; Corona 2: Opx - Pl; Corona 3: Grt - Qtz+liq; Corona 4: Bt - Pl+Qz	Corona 1: Bt | Grt+Qtz | Pl; Corona 2: Opx | Grt+Qtz+Bt+Pl | Pl; Corona 3: Grt | Crd+Opx+Bt+Pl+Spl symp | Qtz+Melt; Corona 4: Bt | Crd+Opx+Qtz | Pl	Corona thickness: 100 - 200 µm; Vermicule size: 5 - 50 µm; Vermicule spacing: –; Vermicule Shape: Vermicular symplectite; Preferred Orientation: Vermicular symplectite weakly oriented perpendicular to layer boundaries	Coronas 1 and 2: X_{Grs} increases toward Pl (from 2 - 3 mol.% to 3 - 4 mol.%). Opx: Al^{VI} = 0.05 - 0.07 a.p.f.u. and X_{Mg} = 0.59 - 0.63. Corona 3: Grt: Ti = 0.24 - 0.28 a.p.f.u. and Al^{VI} = 0.12 - 0.17 a.p.f.u. Corona 3: Opx: Al^{VI} = 0.08 - 0.12 a.p.f.u. and X_{Mg} = 0.63 - 0.65. Biotite: X_{Mg} = 0.71 - 0.76. No indication of symmetry in zonation.	Coronas 1 and 2: 690 - 790 °C and 7.7 - 9.0 kbar; Corona 3: 900 - 920 °C and 4.3 - 4.7 kbar; Corona 4: 860 - 880 °C and 4.0 - 4.4 kbar (Average PT, THERMOCALC)	Clockwise	SSDC	-	Coronas formed at unique P-T conditions under steady-state conditions during multi-stage metamorphic history. Coronas 1 and 2: decompressive cooling on clockwise path (2000 Ma). Coronas 3 and 4: renewed burial of granulites (220 Ma) on a second clockwise prograde path. Corona phase compositions broadly determined by composition of local reactants.
I07	Ultramafic	Sefuri Mountains, NW Kyushu, Japan	Ol - Pl	Corona 1: Ol | Opx | Pl; Corona 2: Ol | Hbl+Opx | Hbl+Spl symp | Pl	Corona thickness: Corona 1: < 70 µm; Corona 2: < 400 µm; Vermicule size: --; Vermicule Shape: Corona 1: Columnar Opx; Corona 2: Granoblastic polygonal layer 1. Layer 2 comprises vermicular symplectite weakly oriented perpendicular to layer boundaries	At cation total decreases (1.21 - 0.48; 23 O's) and X_{Mg} increases (0.88 - 0.91) in Hbl toward Ol in layer 1. X_{Al} in Opx increases toward Pl (0.06 - 0.11) in layer 1.	600 - 700 °C, 5 kbar (Hbl-Opx thermometry on mineral pairs from layer 2 - employing Gibbs method for Fe-Mg exchange between Hbl and Opx)	Not described	SSDC	-	Open system removal of MgO from the local corona volume, stabilises Opx in the corona.

Table 1 continued: Summary of prograde corona occurrences in the literature

Tag	Bulk comp	Location	Reactants	Corona product assemblage	Corona Thickness, Vermicule size, Vermicule spacing	Equilibration	P, T of corona formation	Inferred P-T path	Layer growth model	Diffusion model	Comments
MCC03	Metapelite	Makhavinesh Lake Pluton	Grt - Qtz-Fsp	Grt | Crd+Opx | Pl | Opx | Qtz+Fsp	Corona thickness: <50 μm (6 km from pluton) to > 1000 μm (adjacent to pluton) Vermicule size: <10 μm (6 km from pluton) to 250 μm (adjacent to pluton) Vermicule spacing: – becoming more equant toward pluton Orientation: Rods strongly aligned perpendicular to gamet substrate	Al₂O₃ wt % and X_Mg of Opx increases toward reactant garnet. Magnitude of difference dependent on distance to pluton. Max ΔAl wt% = 0.8 wt%; Max ΔX_Mg, 0.05. Overall Opx more Fe-rich and Al-rich toward pluton. Intracrystalline zonation toward lower Al wt% and X_Mg values at margins of vermicules.	Grt - Opx. Al-solubility thermometry: Contact: 785 - 875 °C at 5 kbar At 6km: 650 - 750 °C	Contact aureole	SSDC	-	Progressive replacement of gamet toward pluton contact
IOO2	Peltic and mafic granulites	Taylor Brook Gabbro Complex	Corona 1: Sil - Grt - Qtz Corona 2: Grt - Qtz	Corona 1: Grt | Spl + Crd | Qtz+Sil +Grt Corona 2: Grt | Pl | Opx | Qtz	Corona thickness: Corona 1: < 500 μm Corona 2: < 100μm Vermicule size: Corona 1: < 300 μm Corona 2: < 50 μm Vermicule Shape: Corona 1: Tortuous, contorted lamellar symplectite Corona 2: Granoblastic-polygonal Orientation: Lamellae weakly aligned perpendicular to gamet substrate	No zonation described.	Grt-Opx-Pl-Qtz thermobarometry on corona phases in metabasite yields a P-T estimate of 4.4 kbar at 615°C. Coronas in tonalitic gneiss yield a slightly higher P and T of 4.7 kbar at 645°C.	Contact aureole	SSDC	-	-
BBOO	Metapelite	Mafic Complex Contact Aureole	Crd - Kfs	Crd | Bt+Sil+Qtz | Kfs	Corona thickness: < 200μm Vermicule size: <30 μm Vermicule spacing: > 5 μm Vermicule Shape: Vermicular symplectite	No zonation described.	-	Contact aureole	-	-	-
WMP04	Metapelite	Ross of Mull Contact Metamorphic Aureole, Scotland	Corona 1: Ky - Bt - Qtz Corona 2: Grt - Qtz - Ms	Corona 1: Ky | Crd + Ms | Qtz+Bt Corona 2: Grt | Crd + Bt | Qtz+Ms	Corona thickness: Corona 1: < 350 μm Corona 2: < 1000μm Vermicule size: Corona 1: - Corona 2: < 20 μm Vermicule Shape: Corona 1: Fibrous intergrowth Corona 2: Elongate, anhedral biotite laths in cordierite Orientation: Vermicules weakly aligned perpendicular to reactant substrate	Zonation not described. Apparently in equilibrium.	P-T estimates based on relative stability of phases on P-T grids	Contact aureole	-	-	=
L04	Metatroctolite	Back Creek Ultramatic body, North Carolina Blue Ridge	Ol - Pl	Ol | Opx | Cpx+Spl symp | Pl Ol | Opx | Cpx+Hbl symp | Pl Ol | Opx | Cpx+Spr symp | Pl	Corona thickness: 0.5 - 0.75 mm Vermicule size: -- Vermicule Shape: Vermicular symplectite and elongate or columnar Opx laths Orientation: Strongly oriented perpendicular to layer boundaries	Equilibrium. No variation in composition.	700 - 900 °C and > 9 kbar	-	SSDC	Closed. No diffusion modelling performed. SVD analysis concludes Hbl of primary metamorphic origin - not retrograde after Cpx.	Overall corona reaction modelled by SVD (Singular Value Decomposition) matrix technique. Possible mass balance reactions are generated by SVD technique. A successful model is one that reproduces a sensible overall reaction with residuals that match expected analytical errors (Lang et al., 2004). Closed system approximation possibly invalid.

Table 1 continued: Summary of prograde corona occurrences in the literature

Tag	Bulk comp	Location	Reactants	Corona product assemblage	Corona Thickness, Vermicule size, Vermicule spacing	Equilibration	P, T of corona formation	Inferred P-T path	Layer growth model	Diffusion model	Comments
DO2	Mafic granofels	Arthur River Complex at Mt Daniel, Fiordland, New Zealand	Hbl - Czo	Hbl [Cpx + Ky + Qtz + Pl [Czo	Corona thickness: < 500 μm Vermicule size: < 60 μm Vermicule spacing: -- Vermicule Shape: Irregular, elongate, euhedral laths of Ky embedded in Cpx and Qtz. Orientation: No preferred orientation	No zonation - equilibrium.	The assemblage garnet, kyanite, plagioclase and quartz yielded pressure estimates of 13.2 kbar and temperature estimates of 700 °C using conventional thermobarometer of Newton and Perkins, 1982.	Contact aureole	-	-	-
D97	Metapelite	Chimakurthy mafic-ultramafic complex aureole, Eastern Ghats Belt, India	Spl - Crd	Corona 1: Spl [Grt + Sil + Crd [Crd Corona 2: Grt [Opx + Sil + Spl	Corona thickness: Corona 1: < 75 μm; Corona 2: < 230μm Vermicule size: Corona 1: < 15 μm; Corona 2: < 10 μm Vermicule spacing: -- Vermicule Shape: Corona 1: Irregular, lenticular sillimanite needles in cordierite intergrown with 'spongy' garnet Corona 2:Rod-like intergrowth of Opx, Sil and Spl Orientation: Orthopyroxene vermicules aligned perpendicular to layer boundaries	No zonation described.	P-T grid constraints on pressure: 5 - 6 kbar with cooling from 1000 °C.	Contact aureole	-	-	-

JC90: Johnson and Carlson, (1990); N83: Nishiyama, (1983); J04: Johnson et al., (2004); WC97: White and Clarke, (1997); I93: Indares, (1993); JF88: Joesten and Fisher, (1988); ABE92: Ashworth et al., (1992); K87: Koons et al., (1987); WM83: Whitney and McLelland, (1983); A98: Ashworth et al., (1998); B01: Bruno et al., (2001); WM73: Whitney and Mclelland, (1973); A01: Abart et al., (2001); BB88: Boullier and Barbey, (1988); C06: Chen et al., (2006); I07: Ikeda et al., (2007); MCC03: Mcfarlane et al., (2003); IOO2: Ings and Owen, (2002); BB00: Barboza and Bergantz, (2000);WMP04: Wheeler et al., (2004); L04: Lang et al., 2004; D02: Daczko et al., (2002); D97: Dasgupta et al., (1997).

Appendix 2.

Table 2: Summary of retrograde corona occurrences in the literature

Tag	Bulk comp	Location	Reactants	Corona product assemblage	Corona Thickness, Vermicule size, Vermicule spacing	Equilibration	P, T of corona formation	Inferred P-T path	Layer growth model	Diffusion model	Comments
CP91	Metagabbro	Llano Uplift, Central Texas	*Corona 1:* Grt - Qtz; *Corona 2:* Grt - Omp	*Corona 1:* Grt | Pl+Mg‡ | Opx+Aug | Qtz; *Corona 2:* Grt | Pl+Prg symp | Mg-Hbl | Pl+Mg-Hbl+Opx symp | Omp	*Corona 1:* Corona thickness: Pl = 60 μm; Opx+Hbl = 20 μm; Vermicule size: < 5 - 10 μm; Vermicule spacing:--; Vermicule Shape: Pl+Mg‡ - granoblastic-polygonal; Opx+Aug - columnar; Orientation: Columnar Opx+Aug perpendicular layer boundaries. *Corona 2:* Corona thickness: 200 μm; Vermicule size: < 2 μm - 40 μm; Vermicule Shape: Granoblastic-polygonal Pl; vermicular rod-like Hbl and Opx; Orientation: Weakly perpendicular to layer boundaries	Disequilibrium. Pl less calcic and amphibole Fe/Mg and Al/Si ratios decrease toward quartz/omphacite (An58- An62).	-	ITD	SSDC	Open Grt-Qtz: $L_{Pl} > L_{Aug} \geq L_{Qz} \geq L_{Al} \geq L_{Mg}$; Grt-Omp: $L_{Pl} = L_{Pl} > L_{Aug} \geq L_{Qz} \geq L_{Al}$	-
CPC89	Metapelite	MacRobertson Land, Antarctica	*Corona 1:* Crd - Spl; *Corona 2:* Spl - Matrix (Grt+Sil+Qtz+Kfs); *Corona 3:* Ilm - Grt	*Corona 1:* Spl | Mg‡ | Sil |, Crd; *Corona 2:* Spl | Grt+Sil+Crd | Grt+Sil+Qtz+Kfs; *Corona 3:* Ilm | Sil | Grt	Corona thickness: *Corona 1:* 200 μm; *Corona 2:* < 120 μm; *Corona 3:* 30 - 120 μm; Grain size: < layer thickness; Grain shape: Granoblastic-polygonal; Orientation: None	-	-	IBC following ITD	SSDC	-	-
IG13	Metapelite	Mather Paragneiss, Rauer Group, Antarctica	*Corona 1:* Grt - Qtz; *Corona 2:* Grt - Bt; *Corona 3:* Sil - Opx	*Corona 1:* Grt | Crd+Opx symp | Opx | Qtz; *Corona 2:* Grt | Crd+Opx symp | Pl | Bt; *Corona 3:* Sil | Crd | Opx	Corona thickness: < 0.5mm; Grain size: --; Grain shape: --; Orientation: Symplectite phases perpendicular to layer boundaries	Disequilibrium. Crd X_{Mg} varies across symplectite – generally not systematically, but X_{Mg} may increase toward Opx. No variation in Opx composition.	750 - 800 °C and 7 - 8 kbar, (modal P-T-X relationships from pseudosections)	Decompressive cooling on clockwise path	SSDC	-	-
WPC02	Fe-rich metapelites	Musgrave Block, Central Australia	Grt - Matrix (Sil, Qtz, Kfs, Bt)	Grt | Spl+Qtz+Grt | Matrix; Grt encloses Spl in corona	Corona thickness: < 0.5mm; Grain size 0.05 - 0.2 mm; Grain shape: Granoblastic-polygonal/interlobate; Orientation: None	Equilibrium.	800 - 850 °C and 5.5 - 6.0 kbar (P-T-X relationships from pseudosections)	Clockwise path with minor decompression dominated by cooling	SEQ	-	Coronas develop in response to changing modes in a high variance equilibrium assemblage. No univariant reaction is crossed. Garnet is still stable. Implies that decompression implied by this texture may have been over-estimated in other terranes (Harley, 1989).
KS99	Mg-rich metapelites	Highland Complex, Hakurutale, Sri Lanka	*Corona 1:* Grt - Qtz; *Corona 2:* Grt - Qtz; *Corona 3:* Grt - Bt; *Corona 4:* Sil - Opx+Grt (SiO₂ Deficient EBC)	*Corona 1:* Grt | Opx+Sil symp | Opx | Qtz; *Corona 2:* Grt | Opx+Crd+Spr symp | Opx | Qtz; *Corona 3:* Grt | Opx+Pl+Crd symp | Bt; *Corona 4:* Sil | Crd+Spr symp | Crd | Opx|Grt	Corona Thickness: *Corona 1:* < 0.5mm; Grain Size: *Corona 1:* Coarse granoblastic-polygonal grains < 0.2mm; symplectite vermicules: 10 - 50 μm; Grain shape: Symplectic: vermicular; Monomineralic layers: granoblastic-polygonal; Orientation: Symplectic vermicules weakly aligned perpendicular to layer boundaries	Disequilibrium. *Corona 1:* Opx: $X_{Mg} = 0.76 - 0.84$; $X_{Al} = 0.09 - 0.15$; *Corona 2:* Opx: $X_{Mg} = 0.76 - 0.83$; $X_{Al} = 0.12 - 0.17$; No systematic variation noted.	810 °C and 7.5 kbar. TWQ P-T estimate on Grt, Qtz, Opx, Crd assemblage. Assumed Grt + Qtz in equilibrium with products.	Clockwise path with ITD	SSDC	-	-

Table 2 continued.: Summary of retrograde corona occurrences in the literature

Tag	Bulk comp	Location	Reactants	Corona product assemblage	Corona Thickness, Vermicule size, Vermicule spacing	Equilibration	P, T of corona formation	Inferred P-T path	Layer growth model	Diffusion model	Comments
N02	Mafic, aluminous pelites	Thor-Odin Dome, Shuswap metamorphic core complex, British Columbia	Ged - Ky	Ged | Crd | Crd+Spl symp | Crd+Cm symp | Ky	Corona thickness: Layer 1: < 350 µm Layer 2: < 900 µm Layer 3: pseudomorphs kyanite Vermicule size: 25 - 350 µm Vermicule spacing: 20 µm Vermicule Shape: Vermicular symplectite; granoblastic-polygonal/interlobate in Crd moat Orientation: Vermicular symplectite weakly oriented perpendicular to layer boundaries, otherwise none	Equilibrium. No variation in any phases noted.	P < 5 kbar and T ~ 750 °C. Equilibria constrained with TWQ and conventional thermobarometers.	Rapid isothermal decompression on a clockwise path	SSDC	-	
H06	Metapelite	Leverburgh Belt, South Harris, Scotland	Grt - Qtz	Grt | Crd+Opx symp | Opx | Qtz	Corona thickness: Layer 1: < 200 µm Layer 2: < 50 µm Vermicule size: 10 - 50 µm Vermicule spacing: 25 µm Vermicule Shape: Rod-like symplectite; columnar Opx in layer 2. Orientation: Vermicular symplectite weakly oriented perpendicular to layer boundaries	Disequilibrium. No systematic variation described. Opx: y(Opx) = 0.002 - 0.08 X_{Mg} = 0.71 - 0.78 Cordierite: X_{Mg} = 0.89 - 0.92	P ~ 9 kbar and T ~ 870 °C.	Isothermal decompression on anti-clockwise path	SSDC	-	
G80	Metapelite	Enderbyland, Antarctica	Spr - Qtz	Spr | Sil | Opx | Qtz	Corona Thickness: < 0.5mm	-	7 ± 1 kbar, 900 ± 30 °C	Isobaric cooling on anticlockwise path	SSDC	-	-
B04	Troctolitic gabbro	Snowbird Tectonic Zone, Western Canadian Shield	Grt - Cpx	Grt | Opx+Pl symp | Spl+Cpx+Opx symp | Omp Grt | Prg+Pl | Pl | Opx+Pl | Omp	Corona thickness: Layer 1: < 70 µm Layer 2: 20 µm Layer 3: 50 µm Vermicule size: < 50 µm Vermicule spacing: -- Vermicule Shape: Elongate Prg labtis; euhedral Opx rhombs Orientation: Oriented perpendicular to layer boundaries	Disequilibrium. Marked zonation in Pl (Ab_{02} adjacent Grt to An_{46} at corona margin). No variation in amphibole, orthopyroxene or clinopyroxene compositions documented.	850 - 855 °C at 10 - 12 kbar (two pyroxene thermometry) 810 °C and 12 kbar (Grt-Opx-Pl-Qtz equilibria - TWQ, Grt rim and symplectite compositions)	Isothermal decompression on clockwise path	SSDC?	-	Corona mineralogy depends on availability of H_2O to form amphibole. The use of corona plagioclase composition in TWQ thermobarometry may not be valid.
ACK07	Metapelite	NVP (Neocene Volcanic Province), El Hoyazo, Spain	Grt - Matrix (Bt+Sil+Pl)	Grt | Spl+Crd+Kfs+Melt (glass) | Matrix. Pl rinds separate Spl from Crd.	Corona thickness: < 150 µm Vermicule size: < 50 µm Vermicule spacing: -- Vermicule Shape: Euhedral Spl and granoblastic-interlobate Crd Orientation: No preferred orientation	Equilibrium. No systematic variation in spinel or cordierite composition.	820 ± 50 °C, 4.5 ± 0.6 kbar (ternary feldspar thermometry, Grt-Crd thermobarometry, GASP barometry)	Rapid decompression during eruption followed by isobaric cooling	SSDC/SEQ	-	Plagioclase rind between cordierite and spinel is attributed to isobaric cooling post-eruption.
T06	Metapelite	Mather Paragneiss, Rauer Group.	1) Grt 2) Grt - Melt 3) Sil - Opx 4) Grt - Qtz 5) Grt - Cpx+Hbl	1) Grt | Spr+Opx+Crd symp 2) Grt | Bt+Crd symp | Melt 3) Sil | Spr+Crd symp | Opx 4) Grt | Crd+Opx symp | Opx | Qtz 5) Grt | Opx+Pl | Opx+Pl+Mgt | Cpx+ Hbl	Corona 5: Corona thickness: Layer 1: < 2 mm Layer2: 1 mm Grain size: < 0.5 mm Grain shape: Opx is vermicular. Opx is euhedral and columnar Orientation: Symplectitic Spr. Symplectic vermicules strongly aligned perpendicular to layer boundaries	No variation in corona cordierite observed. Symplectic Orthopyroxene: X_{Mg} = 0.71 - 0.72; 4.1 - 4.2 Al_2O_3 wt.%. Symplectic Spr: Si = 1.36 - 1.39 a.p.f.u.	Two groups of post-peak P-T estimates: 980 - 1010 °C (Grt-Opx thermobarometry) and ~10 kbar; ~ 800 °C and ~ 7 kbar (Grt-Bt thermometry).	Clockwise path with near isothermal decompression under ultrahigh T followed by decompression cooling	1-4) SSDC 5) SEQ	-	

Table 2 continued: Summary of retrograde corona occurrences in the literature

Tag	Bulk comp	Location	Reactants	Corona product assemblage	Corona Thickness, Vermicule size, Vermicule spacing	Equilibration	P, T of corona formation	Inferred P-T path	Layer growth model	Diffusion model	Comments
GT2	Olivine pod in anorthosite	Sognefjord and Bergen, Norway	Ol - Pl	*Type 1:* Ol | Opx | Cpx | Grt | Cpx+Spl | Pl; *Type 2:* Ol | Opx | Cpx | Grt+Cpx+Spl | Pl; *Type 3:* Ol | Cpx | Grt+Cpx+Spl | Pl; *Type 4:* Ol | Cpx | Pl | Grt | Pl	Corona Thickness: *Type 2:* Opx: 6 - 15 mm; Cpx: 4 - 6 mm; Grt: 7 - 15 mm; *Type 3:* Opx: 1 cm; Cpx: 5 mm; Grt: 5 - 8 mm; *Type 4:* Opx: 3 mm; Cpx: 1 mm; Grt: 2 mm; Grain size: --; Grain shape: --; Orientation: --	Disequilibrium. *Type 2 coronas:* Bergen: Opx strongly zoned - Al content and X_{Fe} increase from olivine toward Pl. Garnet strongly zoned - Ca decreases and Mg-Fe increases towards Cpx. Sognefjord: All phases homogeneous. *Type 3 coronas:* All phases homogeneous, except garnet where Ca decreases toward Cpx. *Type 4 coronas:* Mg and Ca increase in Cpx toward plagioclase layer. Ca decreases in the garnet layer toward plagioclase layer.	1000 °C and 12 kbar (Grt-Cpx thermometry) Cooling to 800°C	Cooling from peak igneous T at high pressure	SEQ	-	Coronas 1 - 4 are considered to represent transient, increasingly more evolved stages of corona development on the P-T path.
MAS3	Olivine metagabbro	NE. Scotland	Ol - Pl	Ol | Opx | Hbl | Hbl+Spl | An symp | Pl	Corona thickness: Opx: 70 μm; Hbl: 30 μm; Hbl+Spl: 100 μm; Spinel vermicule size: 0.5 - 5 μm (max.30 μm); Vermicule Shape: *Subhedral, columnar Hbl+Opx; Opx: vermicular spinel*; Preferred Orientation: *Perpendicular layer boundaries*	Disequilibrium. Al content and X_{Fe} of Opx and Hbl increase toward Pl reactant. Opx: Al_{tot} = 0.03 - 0.07; X_{Fe} = 0.26 - 0.28; Hbl: Al_{tot} = 2.72 - 2.77; X_{Fe} = 0.28 - 0.26	Amphibolite facies. No quantitative thermobarometry	Cooling from peak igneous T	SSDC	Open: $L_{Fe} \geq L_{Mg} \geq L_{Ca} > L_{Si}$	
G88	Metagabbro	Central Gneiss Belt, Western Grenville Province, Ontario.	Ol - Pl	Ol | Opx | Cpx | ±Amph | Grt | Pl	Corona thickness: Overall: 250 - 500 μm; Vermicule/Grain size: *Not resolvable*; Vermicule spacing: *Not resolvable*; Vermicule Shape: *Granoblastic-polygonal Grt, columnar Cpx and Opx*; Preferred Orientation: *Opx and Cpx oriented perpendicular to layer boundaries*	Disequilibrium. Opx and Cpx zoned w.r.t. Al. Al - increases from 1.4 - 1.8 wt% toward Pl. Variable Si and Al in amphibole (± 2 wt%). Al/Si ratio decreases in the symplectite toward olivine. Garnet compositions are homogeneous.	8 - 10 kbar and 700 - 750 °C from equilibrium assemblages in host gneisses	Cooling from peak igneous T at high pressure	SSDC - with bulk reaction and re-equilibration.	Closed: Cross coefficient terms L_{CaSi} and L_{CaAl} introduced to stabilise garnet in symplectite. Semi-quantitative results only with $L_{Fe} \approx L_{Mg} > L_{Ca} > L_{Al}$, and $L_{Al}/L_{Ca} <$ 6 - 8. $L_{Ca}/L_{Al} <$ 1.5 - 2.0. $L_{Mg}/L_{Ca} <$ 4 - 6	The closed system assumption forced Grant to assume a "fictive" non-stoichiometric plagioclase composition to accommodate excess Ca required to stabilise Cpx-bearing coronas. The garnet layer was not included in the SSDC model since it was believed to post-date the main corona.
J86	Troctolitic gabbro	Risør, Norway	Ol - Pl	Ol | Opx | Opx symp | Hbl+Spl symp | Pl; Ol | Opx | Hbl+Spl symp | Pl	Corona thickness: Opx layer: 72 - 105 μm; Opx+Spl: 10 - 20 μm; Hbl+Spl: 110 - 205 μm; Vermicule size: Spl: 1 - 2 μm; Vermicule spacing:--; Vermicule Shape: *Opx and Hbl: columnar - Spl: needles/rods*; Orientation: *Spl rods perpendicular to layer boundaries*	Equilibrium - no variation described.	-	Primary coronas magmatic in origin, followed by secondary solid-state annealing	SEQ	Closed: none stable	Diffusional instability of primary coronas drives secondary annealing to produce stable secondary solid-state coronas. Remodelled successfully by Ashworth (1986), consistent with emplacement into regional metamorphic terranes and cooling from igneous temperatures.
WM73	Metagabbro	Adirondacks, New York	Ol - Pl	Adirondack Highlands: Ol | Opx | Cpx | Pl | Grt(+Cpx+Hbl) | Pl	Corona thickness: Overall: 500 - 700 μm; Vermicule/Grain size: *not resolvable*; Vermicule spacing: *not resolvable*; Vermicule Shape: *Granoblastic-polygonal Grt, columnar Cpx and Opx*; Preferred Orientation: *Opx and Cpx oriented perpendicular to layer boundaries*	Id/Ts in Cpx decreases from Ol toward Pl (ascribed to formation under different P-T conditions in sequential model). No variation in X_{Mg} of pyroxenes.	Adirondack Highlands: ~8 kbar and 800°C	Cooling from peak igneous temperatures	SEQ	-	Close association of metagabbros with anorthosite argues against depression of relatively buoyant crust to depths sufficient to explain prograde formation of coronas. Garnet-bearing coronas in the Northern Adirondacks reflect higher pressures during corona formation. Absence of garnet locally in coronas is attributed to kinetic nucleation constraints.

Table 2 continued: Summary of retrograde corona occurrences in the literature

Tag	Bulk comp	Location	Reactants	Corona product assemblage	Corona Thickness, Vermicule size, Vermicule spacing	Equilibration	P, T of corona formation	Inferred P-T path	Layer growth model	Diffusion model	Comments
D89	Metapelite	Central Zone, Limpopo Belt, Zimbabwe	*Corona 1:* Grt - Krn *Corona 2:* Crn - Krn *Corona 3:* Crn - Ged	*Corona 1:* Grt | Ged+Spl | Ged+Spr | Spr+Crd | Krn *Corona 2:* Crn | Spl | Spr+Crd | Krn *Corona 3:* Crn | Spl | Spr+Crd | Ged	Corona thickness: *Corona 1:* *Layer 1:* < 200μm; *Layer 2:* ~ 250 μm; *Layer 3:* < 200 μm *Corona 2:* < 750 μm *Corona 3: Layer 1:* < 1000 μm; *Layer 2: 500 μm; Layer 3:* < 700 μm Grain size: < maximum layer thickness Grain shape: *Symplectite:* vermicular *Monomineralic layers :* granoblastic-polygonal Orientation: *Symplectite vermicules radially aligned in sectors (not always perpendicular to layer boundaries)*	Equilibrium: No variation described in any phases.	700 - 800 °C; 3.5 - 5 kbar (MASH equilibria: Grt-Spr-Spl-Crd thermobarometry)	Isothermal decompression	SEQ	-	-
LAL87	Metapelite	Paderu, Southern India	*Corona 1:* Spr - Qtz *Corona 2:* Spl - Qtz *Corona 3:* Spr - Sil *Corona 3:* Opx - Melt	*Corona 1:* Spr | Sil | Opx/Crd | Qtz *Corona 2:* Spl | Spr | Sil | Qtz Spl | Spr | Opx | Qtz Spl | Sil | Opx | Qtz Spl | Spr | Sil | Grt/Opx | Qtz *Corona 3:* Spr | Opx | Sil *Corona 4:* Opx | Bt+Qtz symp | Melt	-	No systematic variation recorded for any corona phases.	900 ± 60 °C and 6.5 ± 0.7 kbar to 760 ± 50°C and 5.0 ± 0.6 kbar (Grt-Opx thermobarometry) and relationships on the FMASH petrogenetic grid	Decompressive cooling on clockwise path.	SSDC	-	Variation in corona mineralogy dependent on topology of petrogenetic grid and local variation in bulk composition (H$_2$O, P$_{Fe3O4}$ and P$_{O_2}$).
O04	Metapelite	Kontum Massif, Central Vietnam	Grt - Qtz	Grt | ±Prp±Spl symp | Crd+Opx symp | Opx | ±Pl±Kfs | Qtz	Corona thickness: *Symp layer:* < 400 μm; *Mono Opx:* < 100 μm Vermicule size: 20 - 100 μm Vermicule spacing: 10 - 30 μm Vermicule Shape: *Symplectite:* vermicular *Monomineralic Opx:* Columnar/blocky; *Spl:* needles/rods Orientation: *Weakly oriented perpendicular to layer boundaries*	Disequilibrium. Zonation noted but not described Symplectite Opx: X$_{Mg}$= 0.62 - 0.70; 5.8 - 7.6 Al$_2$O$_3$ wt% Crd: X$_{Mg}$= 0.82 - 0.84 Spl: X$_{Mg}$= 0.67 - 0.71 Mono Opx: X$_{Mg}$= 0.67 - 0.71; 4.7 - 5.3 Al$_2$O$_3$ wt%	Cooling from 9 kbar, 1000 °C to 6.5 kbar, 800 °C from FMASH petrogenetic grid, X$_{Al}$ and X$_{Mg}$ contours	ITD on clockwise path	SEQ	-	Assumed preserved metastable equilibria in corona represent discrete P-T conditions.
T04	Metapelite	Gangavarapati, Southern India	*Corona 1:* Grt - Matrix *Corona 2:* Grt - Qtz	*Corona 1:* Grt | Opx+Spr+Spl | Matrix (composite symplectite) *Corona 2:* Grt | Opx+Crd | Qtz	Corona Thickness: *Corona 1:* < 300 μm *Corona 2: Layer 1:* < 1000 μm Grain size: 50 - 100 μm Grain shape: *Symplectite: needle-like Spr rods* *Monomineralic layers:* granoblastic-polygonal Orientation: *Symplectite Spr vermicules strongly aligned radially w.r.t layer boundaries Opx vermicules perpendicular to layer boundaries*	Near equilibrium. Minor asymmetrical zonation in cordierite described with highest X$_{Mg}$ values adjacent to garnet (X$_{Mg}$: 0.85 - 0.89). Spr X$_{Mg}$: 0.73 - 0.75 Spl X$_{Mg}$: 0.41 - 0.44 Opx in corona 1: Al$_2$O$_3$ contents 7.6 - 8.2 wt%. Opx in corona 2: Al$_2$O$_3$ contents 6.9 - 7.5 wt%.	Crd-Opx symp: 950 - 990 °C; > 8kbar Crd-Spr-Spl symp: 850 - 900 °C; 8 kbar (X$_{Mg}$ and X$_{Al}$ Opx thermobarometry, Hensen and Harley, 1990)	Steep decompressive cooling on clockwise path	SSDC	-	-

Table 2 continued: Summary of retrograde corona occurrences in the literature

Tag	Bulk comp	Location	Reactants	Corona product assemblage	Corona Thickness, Vermicule size, Vermicule spacing	Equilibration	P, T of corona formation	Inferred P-T path	Layer growth model	Diffusion model	Comments
ZIB07	Metapelite	Vestfold Hills, East Antarctica	*Corona 1:* Pl - Opx *Corona 2:* Grt - Pl	*Corona 1:* Pl ǀ Pl ǀ ±Kfs ǀ Grt₈₅+Qtz ǀ Opx *Corona 2:* Grt ǀ Grt₄₅+Qtz ǀ Pl	Corona Thickness: *Corona 1:* Layer 1: ? Layer 2: < 40 µm Layer 1: < 170 µm *Corona 2:* Layer 1: < 100 µm Grain size: 5 - 100 µm Grain shape: *Symplectite:* granoblastic *Monomineralic layers:* granoblastic-polygonal Orientation: *Symplectite vermicules weakly aligned perpendicular to layer boundaries*	Grt₁ zoned radially w.r.t. Cu, Fe and Mg. Alm₀.₆₀Grs₀.₁₅ Prp₀.₂₅ ₋ Spt₀.₀₅ with X₈₅ of 0.21 - 0.24.	600 - 680 °C, 6 - 8 kbar (Garnet-Opx thermometry, GAFS barometry)	Isobaric cooling	SSDC	-	-
M98	Fayalite granites	Lofoten Islands, Norway	*Corona 1:* Fa/Mgt - Pl *Corona 2:* Fa/Mgt - Kfs	*Corona 1:* Fa ǀ Opx ǀ Grt+Opx ǀ Pl/Kfs *Corona 2:* Fa ǀ Opx ǀ Amph ǀ Pl/Kfs (Opx+Grt layers thinner and Opx-Grt in Opx-Grt layer is higher adjacent to Kfs than Pl) Mgt ǀ Grt+Opx ǀ Fsp Mgt ǀ Amph ǀ Fsp	Corona Thickness: *Corona 1:* Layer 1: < 50 µm Layer 2: < 20 µm Layer 3: < 20 µm Grain size: 2 - 20 µm Grain shape: *Symplectite:* granoblastic *Monomineralic layers:* polygonal granoblastic Orientation: *Symplectite vermicules aligned perpendicular to layer boundaries*	Disequilibrium. Garnet only exhibits zonation, becoming more calcic (X_{Grs}: 0.09 - 0.15) and magnesian (X_{Mg}: 0.95 - 0.97) toward feldspar.	780 - 840 °C and 4 - 10 kbar (Grt-Cpx-Opx-Pl thermobarometry). Large variation in pressure is due to variation in garnet composition across the corona.	Cooling from peak igneous temperatures	SSDC	Open system model with constant volume constraint: L₄₀>L_{Mg}>L_{Fe}>L_{Ca} > L_{Ca}>L_{Mn}>L_{Si}	Markl et al. (1998) is first study to constrain relative diffusion coefficients of major components in granulite facies granitic rocks.
BPS87	Metapelite	Errabiddy, Western Australia	*Corona 1:* Grt - Ged *Corona 2:* Ky - Ged	*Corona 1:* Grt ǀ Grt+Ged₂ ǀ Ged *Corona 2:* Ky ǀ Stl ǀ Crd ǀ Ged	Corona thickness: < 100 µm Grain size: 20 µm Grain shape: *Symplectite:* granoblastic *Monomineralic layers :* granoblastic-polygonal Orientation: *Symplectite vermicules aligned perpendicular to layer boundaries*	*Corona 1:* X_{Fe} in Crd decreases from 0.17 near Grt to 0.1 - 0.13 adjacent to Ged. Ged X_{Fe} 0.37 - 0.47; Al^{IV} 1.3 - 2.2. *Corona 2:* X_{Fe} in Crd increases toward Ged from 0.10 to 0.16. Ged X_{Fe} 0.26 - 0.36	600 - 650°C, 4 - 6 kbar (P-T-X phase equilibria)	Clockwise reheating of originally high-grade rocks, followed by isothermal uplift	SSDC	-	Variations in the proportions of cordierite and staurolite are directly related to the X_{Fe} and Ca composition of gedrite reactant.
BKC03	Metapelite	Epupa Complex, NW Namibia	Grt - Qtz	Grt ǀ Crd+Opx ǀ Pl ǀ Opx ǀ Qtz	Corona thickness: Layer 1: < 250 µm Layer 2: < 70 µm Layer 3: 20 - 250 µm Grain shape: *Symplectite - lamellar* Orientation: *Symplectite vermicules aligned perpendicular to layer boundaries*	Opx X_{Al₂} increases toward Grt (Al_{tot} 0.12 - 0.25). X_{Mg} of Opx and Crd decrease toward Qtz (0.66 - 0.52 in Opx. 0.87 - 0.81 in Crd) No zonation in Pl.	Stage 1 corona formation: 940 ± 30 °C and 8 ±2 kbar (Grt-Opx thermometry and Grt-Opx-Pl-Qtz barometry on Grt rim, layer 2 Pl and layer 3 Opx) Stage 2 corona growth: 800 ± 60 °C and 6 ±2 kbar (Grt-Opx thermometry and Grt-Opx-Pl-Qtz barometry)	Post peak decompression, followed by near isobaric cooling - clockwise retrograde path	SEQ	-	Increase in Al content in Opx toward Qtz inconsistent with diffusion controlled growth, i.e., Al diffusion is rate-limiting. Either Al diffused anomalously quickly in this instance or the Crd+Opx symplectites formed at lower temperature. Thermobarometry potentially applied to disequilibrium compositions.
TM85	Emeries	Cortland Complex, New York	Spr - Qtz	Spr ǀ Opx ǀ Sil ǀ Qtz	Corona thickness: < 60 µm Grain size: < 60 µm Grain shape: *Granoblastic-polygonal* No preferred orientation	Disequilibrium. Homogeneous Fe-Mg in Opx. Al content in Opx increases toward Spr.	-	-	SEQ	-	Partial equilibrium attained by Fe+Mg, i.e., inferred to be the most rapidly diffusing components such that chemical potential gradients were eliminated

Table 2 continued: Summary of retrograde corona occurrences in the literature

Tag	Bulk comp	Location	Reactants	Corona product assemblage	Corona Thickness, Vermicule size, Vermicule spacing	Equilibration	P, T of corona formation	Inferred P-T path	Layer growth model	Diffusion model	Comments
TVR06	Metapelite	Central Zone, Limpopo Belt, Zimbabwe	Sil - Ged	*Sil* | Spr+Spl+Crd | Crd | *Ged*	Corona Thickness: *Corona 1:* *Layer 1:* <100 µm *Layer 2:* <200 µm Grain size: <100 µm Grain shape: *Symplectite:* needle-like Spr rods *Monomineralic layers :* granoblastic-polygonal/interlobate Orientation: *Symplectite Spr vermicules strongly aligned radially w.r.t. layer boundaries*	Equilibrium. Negligible compositional variation described.	500 - 570 °C, 4 - 6 kbar (X_Fe in Opx; Grt-Crd thermobarometry)	Clockwise decompressive cooling	SSDC	-	-
HM96	Metapelite	Central Zone, Limpopo Belt, Botswana	*Corona 1:* Sil - Opx *Corona 2:* Grt - Qtz	*Corona 1:* *Sil* | Spr+Crd symp | Crd | *Opx* *Corona 2:* *Grt* | Opx+Crd symp | *Qtz*	Corona thickness: *Central Layer 1:* < 80 µm; *Layer 2:* < 400 µm *Corona 2:* < 500 µm Vermicule size: *Corona 1:* not resolvable *Corona 2:* 50 - 200 µm Vermicule spacing: *Corona2:* ~20 µm. Vermicule Shape: *Symplectite phases:* vermicular *Monomineralic layers:* granoblastic-polygonal Orientation: *Spr rods radially oriented w.r.t. layer boundaries* *Opx vermicules perpendicular to layer boundaries*	No systematic variation recorded for any phases. *Corona 2:* Symplectite Opx: X_Mg= 0.68 - 0.75; 4 - 9.0 Al₂O₃ wt% Crd: X_Mg = 0.85 - 0.89	~ 800 °C and 4 - 6 kbar (Grt-Opx thermometry; FMASH P,T grid)	Isothermal uplift followed by isobaric cooling	SSDC	-	-

CJ91: Carlson and Johnson, (1991); CPG89: Clarke et al., (1989); K03: Kelsey et al., (2003b); WPC02: White et al., (2002); KS99: Kriegsman et al., (1999); N02: Norlander et al., (2002); H06: Hollis et al., (2006); G80: Grew, (1980); B04: Baldwin et al., (2004); ACK07: Alvarez-Valero et al., (2007); T06: Tong and Wilson, (2006); G72: Griffin, (1972); MA83: Mongkoltip and Ashworth, (1983); G(88): Grant, (1988); J86: Joesten, (1986); WM73: Whitney and Mclelland, (1973); D89: Droop, (1989); LAL87: Lal et al., (1987); O04: Osanai et al., (2004); T04: Tamashiro et al., (2004); ZH07: Zulbati and Harley, (2007); M98: Markl et al., (1998); BPS97: Baker et al., (1987); BKO03: Brandt et al., (2003); TM85: Tracey and McLellan, (1985); TVR06: Tsunogae and Van Reenen, (2006); HM96: Hisada and Miyano, (1996).